Boundary-Layer Meteorol (2009) 131:193–222
DOI 10.1007/s10546-009-9359-5

ARTICLE

# The Budget of Turbulent Kinetic Energy in the Urban Roughness Sublayer

**Andreas Christen · Mathias W. Rotach · Roland Vogt**

Received: 5 September 2006 / Accepted: 5 February 2009 / Published online: 24 February 2009


**Abstract** Full-scale observations from two urban sites in Basel, Switzerland were analysed to identify the magnitude of different processes that create, relocate, and dissipate turbulent kinetic energy (TKE) in the urban atmosphere. Two towers equipped with a profile of six ultrasonic anemometers each sampled the flow in the urban roughness sublayer, i.e. from street canyon base up to roughly 2.5 times the mean building height. This observational study suggests a conceptual division of the urban roughness sublayer into three layers: (1) the layer above the highest roofs, where local buoyancy production and local shear production of TKE are counterbalanced by local viscous dissipation rate and scaled turbulence statistics are close to to surface-layer values; (2) the layer around mean building height with a distinct inflexional mean wind profile, a strong shear and wake production of TKE, a more efficient turbulent exchange of momentum, and a notable export of TKE by transport processes; (3) the lower street canyon with imported TKE by transport processes and negligible local production. Averaged integral velocity variances vary significantly with height in the urban roughness sublayer and reflect the driving processes that create or relocate TKE at a particular height. The observed profiles of the terms of the TKE budget and the velocity variances show many similarities to observations within and above vegetation canopies.

**Keywords** Atmospheric turbulence · Dispersion · Dissipation · Plane mixing layer analogy · Turbulence · Turbulent kinetic energy · Urban canopy · Urban roughness sublayer · Velocity variances

A. Christen (✉)
Department of Geography, Atmospheric Science Program, University of British Columbia, 1984 West Mall, Vancouver, BC V6T 1Z2, Canada
e-mail: andreas.christen@ubc.ca

M. W. Rotach
Federal Office for Meteorology and Climatology, MeteoSwiss, Krähbühlstrasse 58, 8044 Zurich, Switzerland

R. Vogt
Institute of Meteorology, Climatology and Remote Sensing, Department of Environmental Sciences, University of Basel, Klingelbergstrasse 27, 4054 Basel, Switzerland

## 1 Introduction

In urban environments, nearly all human activities take place within a shallow air volume reaching from street level up to roughly two times the average building height. This *urban roughness sublayer* (Rotach 1999) is partially confined to buildings, trees and other objects, including moving vehicles. Flow and turbulence are strongly influenced by the presence of these individual roughness elements.

The urban roughness sublayer is a central domain of interest when modelling air pollution and dispersion in an urban environment. However, this lowest layer of the urban atmosphere violates many assumptions of classical surface-layer simplifications. It is well known that surface-layer scaling even in idealized cases is valid only in the inertial sublayer—for a city, commencing at about two to five times the height of the buildings. The urban roughness sublayer located below shows time-averaged turbulence statistics and flux densities that are vertically and horizontally inhomogeneous (Rotach 1993b; Oikawa and Meng 1995; Kastner-Klein et al. 2001). This fact complicates the modelling of flow, mixing and dispersion in the urban roughness sublayer enormously. Mainly driven by the practical need for air pollution and plume dispersion models, various conceptual and modelling approaches have been developed specifically for the urban roughness sublayer. Recent developments are summarized by Roth (2000), Britter and Hanna (2003) and Belcher (2005).

Any accurate prediction of dispersion within and close to urban canopies is inherently coupled with appropriate modelling of all relevant processes that create, relocate, and dissipate turbulent kinetic energy (TKE) in the urban roughness sublayer (Rotach et al. 2004). A careful analysis of the terms in the budget equation of TKE forms a sound basis for the discussion of observed velocity variances as well as future model improvements.

In field studies it is difficult to obtain solid estimates of the relevant terms of the TKE budget, and this is, in particular, challenging in a complex setting such as that encountered in the urban roughness sublayer. Nevertheless, there are several physical scale studies addressing the TKE budget in urban-like model canopies (Raupach et al. 1986; Poggi et al. 2004), and together with field measurements from vegetation canopies (Leclerc et al. 1990; Meyers and Baldocchi 1991; Frenzen and Vogel 2001) they provide insight into processes relevant for rough and porous surface–atmosphere interfaces in general. However, the density, the non permeability, clustering and stiffness of buildings that characterize most obstacles in a real urban canopy compared to the flexible, porous and highly fractal structures that are present in vegetation canopies do not imply a direct applicability of results from vegetation canopy studies to urban environments.

## 2 Theoretical and Conceptual Framework

The preferred level of detail where urban near-field dispersion models and urban canopy parameterizations are used is the *neighbourhood scale*, which corresponds to a horizontal resolution of $10^2$–$10^3$ m. Our ability to directly simulate mean flow and turbulence statistics with buildings resolved at that scale is computationally intensive (or impossible), and often not required for many applied problems related to dispersion. Therefore, horizontal homogeneity is conceptually restored in the urban 'canopy' by horizontally averaging over a homogeneous area of the city on the neighbourhood scale, i.e. large enough to include several repetitive building blocks. The canopy approach relies on the horizontal randomness of the flow and turbulence field at larger scales, but individual buildings and street canyons are not resolved in this canopy approach. The canopy approach operates with horizontally averaged

statistics within the roughness sublayer and has been widely used to describe mean flow and turbulence within vegetation canopies (Finnigan 2000).

### 2.1 Horizontal Spatial Averaging

In analogy to vegetation canopies, we denote the horizontal spatial average of any variable $a$ within an indefinite slice of the urban roughness sublayer by angle brackets:

$$\langle a \rangle(z) = \frac{1}{\mathcal{L}\Lambda_a} \iint_{\mathcal{L}} I(x, y, z)\, a(x, y, z)\, \mathrm{d}x\, \mathrm{d}y, \tag{1}$$

where the horizontal area of integration $\mathcal{L} = \mathcal{L}_x \mathcal{L}_y$ must be larger than the characteristic length scales of the urban surface in the $x$- and $y$-directions, $L_x$ and $L_y$. In the case of a city, this corresponds usually to repetitive building blocks that are in the order of 50–500 m. $I(x, y, z)$ is an indicator function, which is 1 if the point lies within airspace, and zero if the point lies within buildings, vegetation or other objects of the urban canopy layer; $\Lambda_a$ is the fractional volume of (outdoor) airspace at a given height-slice in $\mathrm{m}^3\,\mathrm{m}^{-3}$. This implies that in this approach we only consider the 'outdoor air' part of the atmosphere. Strictly speaking, buildings contain airspace, but this 'indoor' airspace is assumed to be mechanically and thermally decoupled from the outdoor atmosphere and not of interest in this framework.

Extending the concept of Reynolds decomposition, any variable $a(\mathbf{x}, t)$ at any point $\mathbf{x}$ and time $t$ in the urban roughness sublayer can now be separated into a spatial-temporal mean part, a deviation of the temporal mean from the spatial-temporal mean (dispersive part) and a turbulent part (Raupach and Shaw 1982), namely

$$a(\mathbf{x}, t) = \langle \overline{a} \rangle + \overline{a}''(\mathbf{x}) + a'(\mathbf{x}, t), \tag{2}$$

with the condition

$$\langle \overline{a}'' \rangle = 0. \tag{3}$$

The horizontally-averaged product of two dispersive departures $\langle \overline{a}''\, \overline{b}'' \rangle$ is called a dispersive flux, and does not necessarily vanish.

### 2.2 The Horizontally-Averaged TKE Budget

By first applying temporal and then spatial averaging, the total kinetic energy of a unit mass is split up into a temporal and spatial mean (MKE), a dispersive (DKE) and a turbulent kinetic energy (TKE):

$$\frac{1}{2}\langle u_i u_i \rangle = \frac{1}{2}\left( \langle \overline{u_i} \rangle \langle \overline{u_i} \rangle + \langle \overline{u_i}'' \overline{u_i}'' \rangle + \langle \overline{u_i' u_i'} \rangle \right) \tag{4}$$

where $u_i = \{u, v, w\}$ are the velocity components in the streamwise ($x$), lateral ($y$) and vertical ($z$) directions. In the subsequent analysis, we focus on MKE and TKE only due to experimental restrictions. For horizontal homogeneous conditions on the neighbourhood scale neglecting advection, the TKE budget equation in the urban roughness sublayer can be written as:

$$\frac{\partial \langle \overline{u_i' u_i'} \rangle / 2}{\partial t} = \underbrace{-\langle \overline{u'w'} \rangle \frac{\partial \langle \overline{u} \rangle}{\partial z}}_{Ps} \underbrace{- \left\langle \overline{u'w'}'' \frac{\partial \overline{u}''}{\partial z} \right\rangle}_{Pw} + \underbrace{\frac{g}{T} \langle \overline{w'\theta'} \rangle}_{Pb} + Pt$$
$$\underbrace{- \frac{1}{\Lambda_a} \frac{\partial \Lambda_a \langle \overline{w' u_i' u_i'} \rangle / 2}{\partial z}}_{Tt} \underbrace{- \frac{1}{\Lambda_a} \frac{\partial \Lambda_a \langle \overline{w}'' \overline{u_i' u_i'}'' \rangle / 2}{\partial z}}_{Td} \underbrace{- \frac{1}{\Lambda_a} \frac{\partial \Lambda_a \langle \overline{p'w'} \rangle}{\partial z}}_{Tp}$$
$$\underbrace{+ \nu \frac{\partial^2 \langle \overline{u_i' u_i'} \rangle / 2}{\partial x_j x_j}}_{Tv} - \epsilon. \tag{5}$$

Here, $\theta$ is virtual temperature, $g$ is acceleration due to gravity, $p$ is kinematic pressure, $\nu$ is kinematic viscosity, and $\epsilon$ is the viscous dissipation rate.

Compared to the TKE budget in the surface layer, additional terms arise from the horizontal averaging procedure, namely a dispersive shear production term (wake production, *Pw*) and the dispersive transport term (*Td*). A further term, *Pt*, is introduced for TKE produced by moving vehicles in the street canyon (Sabatino et al. 2003).

In summary, turbulence is locally produced by shear production (*Ps*), wake production (*Pw*), buoyancy production (*Pb*), and moving vehicles (*Pt*). The locally produced TKE can be vertically relocated by turbulent (*Tt*), dispersive (*Td*), pressure (*Tp*), and viscous transport (*Tv*, neglected in the present analysis). Finally, viscous dissipation ($\epsilon$) is always a sink that converts TKE to heat.

In vegetation canopies, where the horizontal-averaging approach has been developed, the volume of trees is much smaller than the total volume of air in the canopy layer. Therefore, changes in the volume of airspace with height are negligible. However, in a city buildings can occupy a significant fraction of the total volume, which typically results in a reduction of the outdoor air volume with depth. In a city, the changes of the fractional volume with height must be taken into account (Ca et al. 2002). This is reflected in Eq. 5 by $\Lambda_a$ in the transport terms *Tt*, *Td*, and *Tp*.

For a particular height $z$ in the urban roughness sublayer we define the fractional volume of (outdoor) airspace by

$$\Lambda_a = \frac{V_a}{V_a + V_b} \tag{6}$$

where $V_a$ is the volume occupied by outdoor air at a given height (i.e. atmosphere in street canyons and backyards) and $V_b$ is the volume of buildings.

The objective of the presented study is to evaluate the magnitude of the different terms in Eq. 5 so as to gain an understanding of the relative importance of processes that create, relocate, and dissipate TKE in the urban roughness sublayer, and to discuss their impact on velocity variances that are used in dispersion modelling.

## 3 Methods

Experimental data from two turbulence profile towers were used to evaluate the magnitude of the different terms in Eq. 5 under a real urban configuration. The experimental activities were part of the Basel Urban Boundary Layer Experiment (BUBBLE), an experiment dedicated to the energetics and dispersion processes in the urban boundary layer by simultaneously

involving different spatial scales and various approaches ranging from field measurements and remote sensing to scale and numerical modelling (Rotach et al. 2005).

### 3.1 Sites and Instrumentation

In contrast to numerical models and wind-tunnel experiments there is no control of the urban structure in a full-scale field campaign. Further, logistics and instrumental limitations restrict our sampling to a few point locations. The present measurement campaign focussed on two typical European street canyons in the city of Basel, Switzerland. Two towers were operated in urban neighbourhoods characterised by three-storey to six-storey attached houses enclosing large inner courtyards. These courtyards are either open (green space, trees) or consist of garages, parking lots and low commercial-industrial buildings (Fig. 1, left). With such a dense urban morphometry a high plan area fraction of buildings $\lambda_P$ is reached and only a small fraction of the surface is covered by permeable ground.

Table 1 summarises integral site and surface characteristics of both urban surfaces in the tower footprints. A raster-based digital building model at a horizontal resolution of 1 m (Maier 2005) was used to calculate most parameters given in Table 1. Note that parameters listed in Table 1 do not include urban vegetation. Figure 1 (right) shows profiles of the fractional volume $\Lambda_a$ for the two sites derived from the digital building model, separately for 50 and 250 m radii around the sites. Above the highest roofs, $\Lambda_a$ is one, i.e. there are essentially no buildings higher than 25 m (except for two high-rise buildings, see below). At ground level ($z = 0$) $\Lambda_a = 1 - \lambda_P$, where $\lambda_P$ is the plan area fraction covered by buildings. The fractional volume of vegetation is assumed to be a negligible part of $V_a$.

#### *3.1.1 Basel-Sperrstrasse (U1)*

A 32-m high triangular lattice tower was erected inside the 13-m wide street canyon 'Sperrstrasse'. The orientation of the street canyon is along the axis 067°–247° (east-north-east to west-south-west), the length of the block where the tower was operated is 160 m, and the street canyon's average width-to-height ratio is $x_c/z_h = 1.0$. The tower was placed at the midpoint of the block and 3 m away from the north wall (Fig. 2, left). The tower supported a profile of six ultrasonic anemometer-thermometers (sonics, labels A–F, Table 2). The sonics A–E were mounted on horizontal booms reaching from the tower into the centre of the street canyon and sonic F was operated on top of the tower. The lower instruments measured inside the northern half of the street canyon ($x/x_c = 0.37$ where $x$: distance to northern wall, $x_c$: street canyon width).

The total height of the tower was $2.2\,z_h$, where $z_h$ is the mean building height calculated as the average height of all buildings weighted by their plan area in a circle of 250 m around the tower. The mean building height $z_h$ might be an underestimation of the aerodynamically relevant building height because the calculation method includes low buildings in the courtyards that are not important in terms of their form drag (e.g. labels 1 and 2 in Fig. 1). From the vertical profile of the fractional volume $\Lambda_a$ in Fig. 1 it is clear that there is a significant number of buildings roofs that are higher than $z_h$.

Buildings on both sides of the street canyon 'Sperrstrasse' have pitched roofs except two flat-roof buildings directly adjacent to the tower on the northern side (label 3 and 4) and two flat-roof buildings close to the two intersections (label 5 and 6). Gable heights reach typically 15 m on both sides. A high pitched roof of 20 m is located directly to the south-east of the tower (label 7).

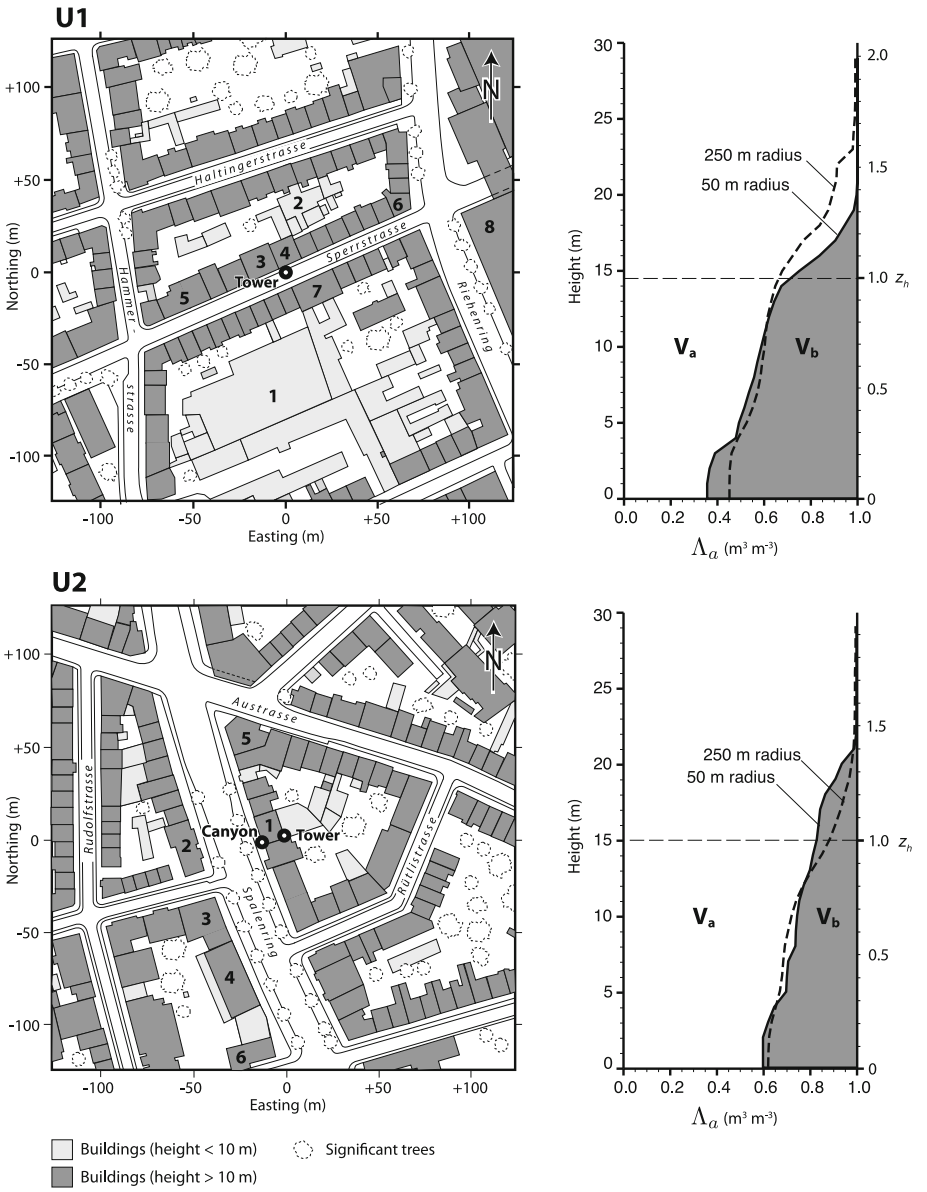


**Fig. 1** *Left*: maps of the urban morphometry around sites U1 (*top*) and U2 (*bottom*). *Right*: vertical profiles of fractional volume $\Lambda_a$ according to Eq. 6 for circles of 50 and 250 m around the sites. $z_h$ is the average building height used in the analysis (see text)

Sectors from west to north-north-east and south-south-east to south-south-west are similar to structure found immediately around the tower. These sectors are surprisingly homogeneous in terms of integral morphometrical statistics and building height. In these sectors the fetch extends up to a minimum of 700 m. In the sector north-east to south-south-east an extensive commercial area is found at 100 m distance to the tower with flat roofs and roof heights from

**Table 1** Site information and integral three-dimensional morphometric parameters of the city surface derived from a raster-based digital building model and aerial photos

| | | U1 | U2 |
|---|---|---|---|
| Name of street | | Sperrstrasse | Spalenring |
| Start of measurement period | | 01 Nov 2001 | 30 Aug 2001 |
| End of measurement period | | 15 Jul 2002 | 19 Aug 2002 |
| Height of tower (m) | | 32 | 38 |
| Mean building height (m) | $z_h$ | 14.6 | 12.5 |
| Standard deviation of roof heights[a] (m) | $\sigma_h$ | 4.9 | 4.1 |
| Frontal aspect ratio | $\lambda_F$ | 0.37 | 0.31 |
| Complete aspect ratio | $\lambda_C$ | 1.92 | 1.75 |
| Local street canyon width to height ratio[b] | $x_c/z_h$ | 1.0 | 1.8 |
| Plan area fraction of buildings | $\lambda_P$ | 0.54 | 0.37 |
| Plan area fraction of vegetated ground | $\lambda_V$ | 0.16 | 0.31 |
| Plan area fraction of impervious ground | $\lambda_I$ | 0.30 | 0.32 |
| Average sky view factor at ground level | $\Psi_{S0}$ | 0.36 | 0.51 |
| Fraction of flat roofs | | 50% | 30% |
| Fraction of pitched roofs | | 50% | 70% |
| Longitude | | 07°35′49″E | 07°34′35″E |
| Latitude | | 47°33′57″N | 47°33′18″N |
| Height of tower base (a.s.l.) (m) | | 255 | 278 |

Values are averages for a circle with 250 m radius around the towers, based on 1 m by 1 m raster elements
[a] Standard deviation of the height of all building raster elements located above 0.5 $z_h$
[b] Value of the local street canyon where measurements are carried out

20 to 25 m (label 8). An isolated high-rise building of 70 m height is located 200 m to the south-west of the tower.

### *3.1.2 Basel-Spalenring (U2)*

In contrast to the tower at U1, the profile of sonics at U2 was not aligned vertically. Three sonics measured within a vegetated street canyon of the avenue 'Spalenring' (A–C, Fig. 2, right) mounted on 4-m booms reaching from balconies of the adjacent building into the street canyon (position $x/x_c = 0.16$ from the eastern wall) while a tower on the roof of the same building supported another three sonics (D–F). The horizontal location of the tower (D–F) is displaced by 20 m to the east (courtyard) relative to sensors A–C. The tower extended the set-up to a height of 38 m above ground (2.5 $z_h$).

The urban morphometry in the footprint of U2 is more complicated than at U1, not only because of the separation of the street canyon and the tower profile, but also because of trees located within the street canyon and a more complex street layout (Fig. 2). The average street canyon width-to-height ratio in the canyon where the measurements were taken is $x_c/z_h = 1.8$. The canyon's orientation is along the axis 169°–349° (south-south-east to north-north-west). There is a major intersection 80 m to the north and two T-intersections at 15 and 60 m to the south of the tower location.

Most buildings along the probed avenue section are pitched roofs except buildings labelled 2–5 that have flat roofs. In contrast to U1, the buildings at U2 show more variability in roof


**Fig. 2** *Left*: photo of the profile tower at U1 taken from inside the street canyon with a view towards WSW. *Right*: photo of the canyon measurements (A–C) and the profile tower (E–F) at U2 taken from roof labelled '4' (see Fig. 1) on the west-side of the canyon towards north

**Table 2** Ultrasonic anemometer-thermometer (sonic) instrumentation, absolute measurement heights $z$, normalized measurement heights $z/z_h$ and fractional volume $\Lambda_a$ according to Eq. 6 in a 50 m radius around the sites

| Site | Code | $z$(m) | $z/z_h$ | $\Lambda_a(z)$ | Instrument type | $F_{\text{out}}$ |
|---|---|---|---|---|---|---|
| U1 | A | 3.6 | 0.25 | 0.43 | Gill R2 Omnidirectional[a] | 20.8 |
| | B | 11.3 | 0.77 | 0.61 | Gill R2 Omnidirectional[a] | 20.8 |
| | C | 14.7 | 1.01 | 0.73 | Gill R2 Omnidirectional | 20.8 |
| | D | 17.9 | 1.23 | 0.95 | Gill R2 Omnidirectional | 20.8 |
| | E | 22.4 | 1.53 | 1.00 | Gill R2 Asymmetric | 20.8 |
| | F | 31.7 | 2.17 | 1.00 | Gill HS | 20.0 |
| U2 | A | 5.6 | 0.37 | 0.70 | Metek USA-1 | 20.0 |
| | B | 13.9 | 0.92 | 0.81 | Metek USA-1 | 20.0 |
| | C | 16.6 | 1.10 | 0.84 | Metek USA-1 | 20.0 |
| | D | 21.8 | 1.44 | 0.99 | Metek USA-1 | 20.0 |
| | E | 29.9 | 1.98 | 1.00 | Metek USA-1 | 20.0 |
| | F | 37.6 | 2.49 | 1.00 | Metek USA-1 | 20.0 |

$F_{\text{out}}$ is the output frequency of the sonic. The capital letters denote corresponding labels in Fig. 1
[a] From May 23 to July 15, 2002 these two instruments were replaced by Metek USA-1 for logistic reasons

height. Generally, buildings along the avenue 'Spalenring' are higher (12–25 m) than buildings along the minor streets (e.g. 'Rütlistrasse' or 'Rudolfstrasse', see Fig. 1). The average building height in a circle of 250 m around the tower is 12.5 m, but this is not representative for the local canyon. The building where the tower is located (pitched roof, label 1 in Fig. 1) extends up to 23 m, and the average height of buildings along the street canyon is 15 m. We therefore used $z_h = 15$ m for U2.

The eastern sector from north to south is homogeneous in terms of morphometry but significantly more vegetated than other sectors. The fetch extends up to a minimum of 600 m. The sector south to south-west incorporates a city park that starts 120 m upwind of U2.

The sector south-west to north has a slightly higher plan area fraction of buildings ($\lambda_P = 0.44$) but a similar mean building height $z_h$ and fetch up to a minimum of 500 m. Two isolated high-rise buildings exist in this area—one 120 m to the south (label 4, height: 42 m) and one 300 m to the north (height: 45 m).

## 3.2 Data Processing

At both sites, wind components $u$, $v$, $w$ and virtual acoustic temperature $\theta$ were continuously recorded at all six levels simultaneously. All data were sampled with an output frequency $F_{\text{out}}$ of 20 or 20.8 $\text{s}^{-1}$ on an on-site computer during the full study period. Data acquisition systems and quality control procedures including wind-tunnel calibrations of the instruments are described and documented in Christen (2005).

### *3.2.1 Frame of Reference*

Flow in the urban roughness sublayer is associated with strong mean vertical velocities and curved streamlines in the mean wind field. Therefore, the widely used double and triple rotation (McMillen 1988), as well as the planar-fit technique (Wilczak et al. 2001), are not suitable as their assumptions are not fulfilled. All instruments were assumed to be correctly aligned. Seven out of 12 instruments were checked on-site with continuously recording inclinometers. Only a single rotation around the vertical $\mathbf{e}_3$-axis into the mean wind at tower top was applied for all levels simultaneously. In this semi-fixed frame of reference, $\mathbf{e}_3$ is always oriented strictly vertical to the surface, $\mathbf{e}_1$ is aligned into the horizontal mean wind at tower top, and $\mathbf{e}_2$ is the resulting lateral component at tower top.

### *3.2.2 Temporal Averaging*

From the time series of $u$, $v$, $w$ and $\theta$ all statistical moments up to order three were calculated and stored for blocks over 60 min. Neither a linear detrending nor any other low-frequency filter was applied. Any detrending algorithm would not ensure that at all tower levels the same amount of energy is removed. This would not only violate energy conservation but also inhibit the possibility of calculating a vertical divergence of any higher-order moment.

### *3.2.3 Horizontal Averaging*

Directly measuring spatial averages of the terms of the TKE budget in a full-scale experiment is nearly impossible, and would require extensive arrays of turbulence sensors. As suggested by Rotach (1993b), a surrogate for a true spatial horizontal average of any term may be approximated from a large ensemble of measured values under different conditions, which reflect different flow configurations. The real horizontal average, deduced from simultaneous measurements at different locations under a particular ambient flow, may converge with the ensemble average of many realisations measured at one location with varying ambient flow. The large dataset collected in this study allows a systematic procedure to retrieve 'horizontally averaged' vertical profiles under different wind directions. The following procedure has been applied to approach the true horizontally-averaged values:

1. The block averages of a time series $\bar{a}(z, t)$ are classified into $N$ equally spaced wind direction sectors $\omega$ based upon wind direction at the tower top.

2. In order to separate the influence of the overall thermal stability, the cases were furthermore binned into ranges of stability as measured at the tower top. Stability was calculated as $\zeta = (z - z_d)/L$ (Garratt 1994), where $L$ is the Obukhov length ($L = \bar{\theta} u_*^2/(k\, g\, \theta_*)$) calculated with both scaling velocity $u_*$ and scaling temperature $\theta_*$ measured at the tower top. It will be shown below that on average at the tower top, turbulence is mainly dependent on shear and buoyancy production and therefore Monin–Obukhov similarity theory is a reasonable approach at this height. Also, $z_d$ is the zero-plane displacement that was set to $z_d = 0.7 z_h$ for all runs at both sites; this value is in the typical range suggested for high-density urban roughness elements with skimming flow (Grimmond and Oke 1999).
   Runs were classified into four ranges, namely *stable* ($+0.1 < \zeta \leq +10$), *near-neutral* ($-0.1 < \zeta \leq +0.1$), *weakly unstable* ($-0.5 < \zeta \leq -0.1$), and *unstable* ($-10 < \zeta \leq -0.5$). Further, runs with $u_* < 0.15\,\mathrm{m\,s^{-1}}$ at tower top were excluded from the analysis (287 h at U1, 466 h at U2). Those low wind speed conditions show high sensitivity to small errors in $u_*$ when scaling terms by $u_*^3$.
3. For each wind direction sector $\omega$, a conditional average $[\bar{a}](\omega, z)$ was calculated from the full time series of $T$-averaged time blocks. The conditional average is denoted by square brackets and describes the average value at a given height under the following conditions,

$$[\bar{a}](\omega, z) = \frac{1}{T\bar{J}} \sum_{t=1}^{T} \bar{a}(t, z) J(t) \tag{7}$$

   where $J(t)$ is an indicator function that is set to 1 if at a given timestep $t$ the average wind vector is from the selected wind direction $\omega$ and set to zero otherwise. $\bar{J}$ is the temporal average of $J(t)$ over the whole dataset and denotes the frequency of wind from the given sector.
4. Finally, the equally weighted average over all $[\bar{a}](\omega, z)$ at a given height $z$ is taken as a surrogate of a horizontal average and is denoted by angle brackets,

$$\langle \bar{a} \rangle(z) = \frac{1}{N} \sum_{\omega=1}^{N} [\bar{a}](\omega, z). \tag{8}$$

   All terms in angle brackets in the present work are calculated with the above procedure, with a resolution of $N = 16$ wind direction sectors.

## 4 Results and Discussion

### 4.1 The Vertical Profiles of MKE and TKE

Figure 3a shows horizontally-averaged profiles of the mean streamwise wind component $\overline{u}$. All individual values were normalised by the streamwise wind component $\overline{u}_0$ at tower top for each run, and the average profiles of $\langle \overline{u}/\overline{u}_0 \rangle$ were then scaled with their value at two times the mean building height $\overline{u}_{2z_h}$. The error bars used in this and all subsequent plots give an indication of the directional variability, and represent the range of the 16 different wind direction bins that are shown in detail for U1 in Fig. 5a. The streamwise wind velocity component varies significantly with different approaching flow conditions. In the street canyons, negative values are observed under cross-canyon flow, corresponding to situations where a

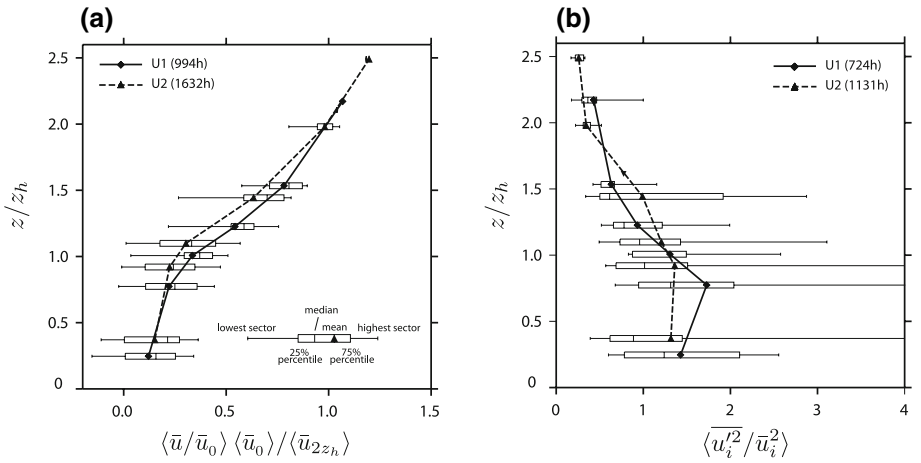


**Fig. 3** Vertical profiles of **a** the normalized streamwise wind component (see text for scaling) and **b** the ratio between TKE and MKE. *Data source*: hourly block averages, November 1, 2001 to July 15, 2002, near-neutral conditions only

street canyon vortex develops and the streamwise component of the flow at the street canyon floor is opposed to that at tower top (recall that the coordinate systems at all heights are globally aligned into the mean wind direction at tower top). Strongest gradients of horizontal wind are observed just above rooftop due to the skimming flow over the rather narrow street canyon. Similarly to profiles measured over and within vegetation canopies (Finnigan 2000), an inflexion point is found slightly above the mean building height $z_h$ at both sites. Finally, the profiles at the topmost sections blend to the logarithmic profile expected in the inertial sublayer above. Feddersen (2005) analysed the neutral wind profile above a scale model of the urban neighbourhood around U1, and his wind-tunnel data suggest a well-defined inertial sublayer above $3.3z_h$ with a logarithmic profile that, on the spatial average, reaches down to $1.6z_h$.

Figure 3b shows vertical profiles of the ratio of the TKE to MKE. In a relative sense, as height decreases, TKE becomes a more important contributor to the total kinetic energy, with the ratio of TKE to MKE reaching its maximum in the upper street canyon. In the lower street canyon air volume, the ratio of TKE to MKE stays roughly constant with depth.

### 4.2 Shear Production *Ps*

Shear production *Ps* is the conversion of mean kinetic energy to TKE due to a gradient in the mean wind associated with turbulent momentum transport (Reynolds stress). In addition to the horizontally-averaged profile of the streamwise wind component $\langle \bar{u} \rangle$, we need information on the Reynolds stress. Figure 5b shows the measured Reynolds stress $\overline{u'w'}$ normalized by $u_*^2$ at tower top for different wind directions observed at U1. Here, and in all the sections below, $u_*$ is the square root of the inertial sublayer value of $\overline{u'w'}$, i.e. the measured $(-\overline{u'w'})^{0.5}$ at tower top. It is thus assumed that the measurements at tower top are close to the inertial sublayer value.

Above the highest roofs, the horizontally-averaged Reynolds stress $\langle \overline{u'w'} \rangle$ is roughly constant with height, so, on the horizontal average, a constant-flux layer is observed. At roof height, $\langle \overline{u'w'} \rangle$ shows a strong reduction in magnitude in the region $1.5 > z/z_h > 0.7$. For all

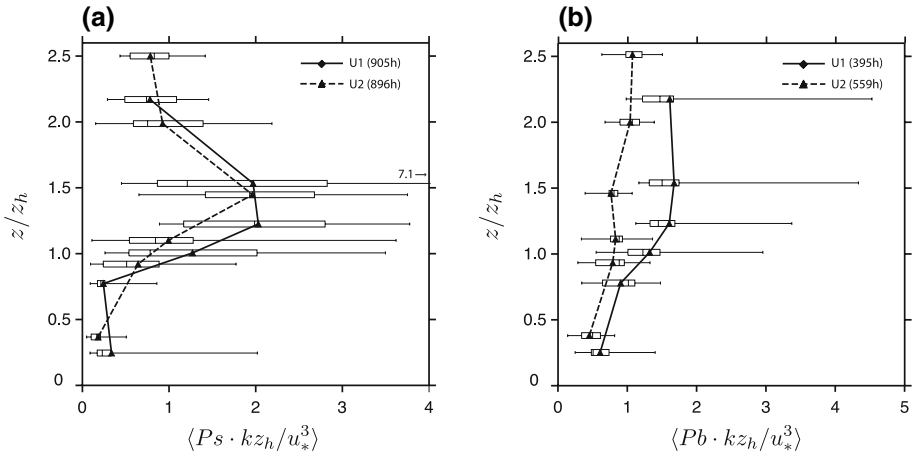


**Fig. 4** Vertical profiles of **a** the normalized shear production term for near-neutral conditions and **b** the normalized buoyancy production term under unstable conditions at tower top. In this and all subsequent figures, $u_*$ is the inertial sublayer value measured at tower top. *Data source*: hourly block averages, November 1, 2001 to July 15, 2002

wind directions observed at U1, the Reynolds stress is negligible in the lower street canyon. The conditional profiles for different wind directions shown in Fig. 5b indicate that there is considerable directional variability, with flow perpendicular to the street canyon characterized by stronger gradients of $\overline{u'w'}$ compared to the along-canyon flow. In particular the high pitched roof to the south-east of the tower (wind from south-east, Label '7' in Fig. 1) creates an extraordinarily strong peak of $\overline{u'w'}$ at the top of the roof (20 m). Flow over the 15-m high flat roofs (wind from north-north-west, Labels '3' and '4' in Fig. 1) shows a steadily increasing $\overline{u'w'}$ with height between $0.75 < z/z_h < 1.5$ without a peak.

Figure 4a shows the resulting turbulent shear production term $Ps$ for near-neutral conditions at both towers. The vertical gradient of wind velocity has been approximated by the local derivative of a parametric cubic spline interpolation with the lower boundary set to zero at $z = 0$ and a relaxed upper boundary at the topmost measurement level (Press et al. 1994). To account for a varying wind direction due to channelling, both horizontal wind components have been taken into account and shear production was calculated from

$$Ps = \left| \overline{u'w'} \frac{\partial \overline{u}}{\partial z} \right| + \left| \overline{v'w'} \frac{\partial \overline{v}}{\partial z} \right|. \tag{9}$$

The shear production term, as have all other terms of the TKE budget in this study, has then been normalised by $kz_h/u_*^3$. On average, shear production, is strongest at the height where most roofs are located in the range $1.2 < z/z_h < 1.5$. Shear production decreases rapidly with decreasing height in the street canyon. The height of strongest shear production, as well as the overall magnitude of the term, depend on the direction of the approaching flow (Fig. 5c). Situations with air flowing originally over the buildings with flat roofs (wind from north-north-west, Labels '3' and '4' in Fig. 1) show their maximum in $Ps$ in the range $1 < z/z_h < 1.2$. Situations where flow first encounters the higher pitched roofs (wind from south-east, Label '7' in Fig. 1) result in a strong elevated shear layer at $z/z_h = 1.5$, with $Ps$ values that are on average more than three times the magnitude compared to those observed for wind from the north-west. If air flows first over the pitched roof row, this results in strong

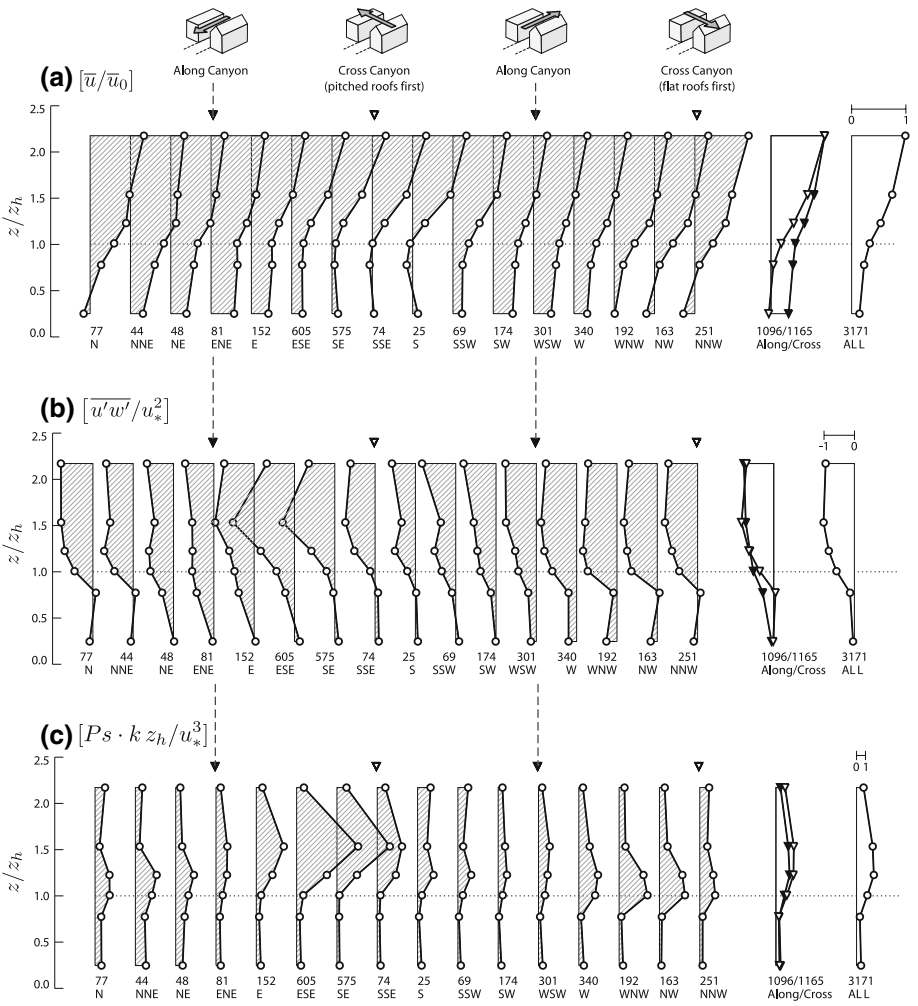


**Fig. 5** Conditionally-averaged profiles of **a** the streamwise wind component $\overline{u}/\overline{u}_0$, **b** local Reynolds stress $\overline{u'w'}$ normalized by $u_*^2$ at tower top, and **c** scaled shear production term $Ps\, k\, z_h/u_*^3$ at U1 for all 16 wind direction classes separately, for conditionally averaged along- and cross-canyon situations, and the 'horizontally-averaged' profile of all 16 classes (*right*) according to the procedure outlined in Sect. 3.2.3. Numbers above the wind direction labels denote the number of hourly blocks included in the conditionally averaged profiles. *Data source*: hourly block averages, November 1, 2001 to July 15, 2002, all stabilities

wind gradients and low $\overline{u}$ in the whole street canyon. Weaker wind gradients are found with flow first over the flat roofs. Along-canyon flow is characterised by slightly smaller shear production rates on average. Similar observations are made at U2 (Fig. 4a and Table 3), where highest values are observed in the range $1.1 < z/z_h < 1.5$. The magnitude of the horizontally-averaged and normalized shear production *Ps* at the two sites is comparable, which is surprising given the fact that the profile at U2 is displaced (street vs. courtyard tower) and hence information extracted from vertical gradients at U2 is limited.

**Table 3** Summary of all production terms in the budget equation of TKE normalized by $k\, z_h/u_*^3$, i.e. shear production *Pb*, wake production *Pw*, and buoyancy production *Pb*

| Site | $z/z_h$ | $\langle Ps\rangle$ | $\langle Pw\rangle$ | $\langle Pb\rangle$ | $\langle Pw\rangle/\langle Ps\rangle$ | $\langle Pb\rangle/(\langle Ps\rangle + \langle Pw\rangle)$ | Cases $\lvert Pb\rvert > \lvert Ps\rvert$ |
|---|---|---|---|---|---|---|---|
| U1 | 2.17 | 0.78 | 0.00 | 0.39 | 0.00 | 0.50 | 10.9% |
| | 1.53 | 1.80 | 0.05 | 0.47 | 0.03 | 0.25 | 17.4% |
| | 1.23 | 1.93 | 0.89 | 0.50 | 0.46 | 0.18 | 27.2% |
| | 1.01 | 1.21 | 0.98 | 0.40 | 0.81 | 0.18 | 25.0% |
| | 0.77 | 0.37 | 0.38 | 0.26 | 1.02 | 0.35 | 23.5% |
| | 0.25 | 0.50 | 0.16 | 0.17 | 0.31 | 0.26 | 24.5% |
| U2 | 2.49 | 0.61 | 0.00 | 0.36 | 0.00 | 0.59 | 15.9% |
| | 1.98 | 0.84 | 0.00 | 0.36 | 0.00 | 0.43 | 7.5% |
| | 1.44 | 2.01 | 1.03 | 0.26 | 0.51 | 0.09 | 13.0% |
| | 1.10 | 1.01 | 0.09 | 0.33 | 0.09 | 0.30 | 22.4% |
| | 0.92 | 0.78 | 0.85 | 0.32 | 1.09 | 0.20 | 21.1% |
| | 0.37 | 0.31 | 0.35 | 0.18 | 1.13 | 0.27 | 29.9% |

*Data source*: Hourly averages, November 1, 2001 to July 15, 2002, all stabilities and flow situations, $n = 3,171$ h (U1) and $n = 3,203$ h (U2)

### 4.3 Wake Production *Pw*

The wake production term *Pw* accounts for turbulence created in the wakes of buildings due to the horizontal variation of the product of mean velocity profile and Reynolds stress. *Pw* could not be measured directly with the current set-up, since in the field this would require a huge array of horizontally separated sensors around buildings, which is impractical. We therefore estimate *Pw* based on Raupach et al. (1986) with the addition that we account for a changing fractional volume $\Lambda_a$ with height and include the divergence of the dispersive stress $\overline{u}''\overline{w}''$

$$-\left\langle \overline{u'w'}'' \frac{\partial \overline{u}''}{\partial z} \right\rangle = \langle \overline{u}\rangle f_F = -\langle \overline{u}\rangle \frac{1}{\Lambda_a}\left( \frac{\partial \Lambda_a \langle \overline{u'w'}\rangle}{\partial z} + \frac{\partial \Lambda_a \langle \overline{u}''\overline{w}''\rangle}{\partial z} \right). \tag{10}$$

This approach assumes that the vertical gradient of Reynolds stress and the vertical gradient of dispersive stress with height are solely attributed to form drag $f_F$ and not to viscous drag. It is further constrained by the assumption that direct dissipation by the building elements from mean kinetic energy to heat without conversion to wake turbulence is negligible and there is no advection. The first term in brackets on the right-hand side contains the divergence of the Reynolds stress that can directly be measured, but the divergence of the dispersive stress was not directly measured. Wind-tunnel studies by Raupach et al. (1986) and Cheng and Castro (2002) both conclude that the dispersive stress $\overline{u}''\overline{w}''$ is insignificant above and in the upper part of canopies. However, recent numerical simulations with urban-like arrays by Coceal et al. (2006) and Martilli and Santiago (2007) show that the dispersive stresses can be very significant within the canopy.

We have estimated $\langle \overline{u}''\overline{w}''\rangle$ for each stability class, based on the following three assumptions: (i) the inertial sublayer starts above $z/z_h = 2$, suggesting that for $\overline{u}_0$ at tower top we can write $\langle \bar{u}_0\rangle = \bar{u}_0$ for all realizations of the approaching flow; (ii) the shape of the horizontally-averaged wind profile does not change with changing wind speed in the given stability class; (iii) different flow configurations found under different wind directions at the

**Table 4** Normalized Reynolds stress $R = \langle \overline{u'w'}/u_*^2 \rangle$ and normalized dispersive stress $D = \langle \bar{u}''\bar{w}''/u_*^2 \rangle$ estimated according Eq. 10, the relative importance of the dispersive stress $|D|/(|R| + |D|)$ and their vertical gradients

| | $z/z_h$ | $R = \langle \overline{u'w'}/u_*^2 \rangle$ | $D = \langle \bar{u}''\bar{w}''/u_*^2 \rangle$ | $\lvert D\rvert/(\lvert R\rvert + \lvert D\rvert)$ | $z_h(\partial R/\partial z)$ | $z_h(\partial D/\partial z)$ |
|---|---|---|---|---|---|---|
| U1 | 2.17 | −1.00 | – | – | – | – |
| | 1.53 | −1.02 | −0.04 | 4% | −0.20 | 0.14 |
| | 1.23 | −0.83 | −0.11 | 12% | −0.88 | 0.16 |
| | 1.01 | −0.58 | −0.13 | 18% | −1.55 | 0.13 |
| | 0.77 | −0.12 | −0.17 | 58% | −1.10 | 0.10 |
| | 0.25 | 0.00 | −0.19 | 100% | −0.11 | −0.36 |
| U2 | 2.49 | −1.00 | – | – | – | – |
| | 1.98 | −0.79 | −0.04 | 5% | −0.04 | −0.02 |
| | 1.44 | −0.89 | 0.03 | 3% | −0.36 | 1.04 |
| | 1.10 | −0.57 | −0.76 | 57% | −0.89 | 0.43 |
| | 0.92 | −0.41 | −0.51 | 55% | −0.75 | −1.15 |
| | 0.37 | −0.06 | 0.03 | 96% | −0.38 | −0.44 |

*Data source*: hourly averages, November 1, 2001 to July 15, 2002, near-neutral runs only, $n = 905$ h (U1) and $n = 896$ h (U2)

tower converge to the spatial average. Based on those three assumptions we approximate the dispersive stress $\langle \bar{u}''\bar{w}'' \rangle$ with the help of the averaged wind profile $\langle \bar{u}/\bar{u}_0 \rangle$:

$$\langle \bar{u}/\bar{u}_0 \rangle(z) \approx \langle \bar{u} \rangle(z)/\bar{u}_0, \tag{11}$$

and

$$\bar{u}'' = \bar{u} - \langle \bar{u} \rangle = \bar{u} - \bar{u}_0 \langle \bar{u}/\bar{u}_0 \rangle(z). \tag{12}$$

Further, mass continuity leads to $\langle \bar{w} \rangle = 0$, and it follows that a measured non-zero vertical mean wind $\bar{w} = \bar{w}''$. Applying the horizontal-averaging procedure described in Sect. 2.1 to $\overline{u}''\overline{w}''$ we are able to estimate the vertical profile of $\langle \bar{u}''\bar{w}'' \rangle(z)$. Table 4 summarizes the estimates for the normalized $\langle \bar{u}''\bar{w}''/u_*^2 \rangle$ in relation to the turbulent Reynolds stress. A dispersive stress is existent and consistently negative at both sites, i.e. the dispersive stress transports momentum downward in the same direction as the Reynolds stress. The dispersive stress $\langle \bar{u}''\bar{w}'' \rangle$ is small above $z_h$, but in the street canyon, the dispersive stress can be of the same magnitude as the Reynolds stress. At the canyon floor the dispersive stress even dominates the weak total momentum exchange, implying physically that flow situations in the street canyon with a mean positive vertical velocity (rising region) have a lower horizontal wind speed than regions with a mean negative vertical velocity (sinking region), which exhibits a greater horizontal wind. Note that the estimated profile of $\langle \overline{u}''\overline{w}'' \rangle$ results in a positive $\langle \partial \bar{u}''\bar{w}''/\partial z \rangle$ (Table 4). As a consequence, the dispersive stress divergence is counter directed to $\langle \partial \overline{u'w'}/\partial z \rangle$; still, $\langle \partial \bar{u}''\bar{w}''/\partial z \rangle$ is in most cases smaller compared to $\langle \partial \overline{u'w'}/\partial z \rangle$.

Practically, $Pw$ was calculated based on the right-hand side of Eq. 10. The divergence of Reynolds and dispersive stress was calculated with the lower boundary set to zero at $z = 0$ and the upper boundary condition at the topmost level to $\partial \langle \overline{u'w'} \rangle/\partial z = 0$ and $\langle \partial \bar{u}''\bar{w}''/\partial z \rangle = 0$. The upper boundary condition is well justified by the profiles of Reynolds stress shown in Fig. 5b and imposed by the assumptions concerning the estimation of the dispersive flux.

Strongest wake production is found at $z_h$ at U1 (Table 3), and at 1.44 $z_h$ at U2, corresponding to the region where $\partial \overline{u'w'}/\partial z$ is strongest and roofs occupy a significant fraction of the volume. In relative terms, the ratio *Pw*/*Ps* decreases with increasing height above the roofs and is highest in the upper street canyons at both sites. This estimation suggests that *Pw* is a non-negligible production term at both sites at roof top and in the street canyon.

### 4.4 Buoyancy Production / Damping *Pb*

Buoyancy production is the process of creating TKE from density differences and rising thermals. It was directly calculated from the kinematic heat flux $\overline{w'\theta'}$ and absolute temperature (Term *Pb* in Eq. 5). At $z_h$, buoyancy production is typically three to five times less important than shear production (Table 3). This is surprising as both sites are characterized by a strong kinematic heat flux $\overline{w'\theta'}$ that stays positive (upward directed) even at night (Christen and Vogt 2004). The relatively small contribution of buoyancy production to the overall TKE in most parts of the profile results in a dominating near-neutral or only slightly unstable urban roughness sublayer. Figure 4b illustrates normalized vertical profiles of *Pb* for unstable runs ($-10 < \zeta < -0.5$), and, unlike *Ps* and *Pw*, *Pb* is approximately constant with height above roofs, indicating a constant-flux layer. From a relative point of view, this suggests that with increasing height above roofs, mechanical production (*Ps* and *Pw*) decreases but buoyancy production *Pb* stays constant, an effect that results in variable dynamic stability with height, i.e. we observe a greater diabatic variation at tower top, where on average *Pb* amounts to 50% of (*Ps* + *Pw*).

Even though roof areas are the major source of sensible heat, *Pb* is a non-negligible term in the upper street canyon. Here, heated canyon walls and the floor contribute to a notable buoyancy production on average. Compared to *Ps* that shows a strong decay with depth and reaches values close to zero in the middle of the street canyon, *Pb* more linearly decays with depth and is still a significant production term at the lowest measurement levels in the street canyon under unstable conditions.

Figure 8a illustrates the horizontal variability of the vertical profiles of $\overline{w'\theta'}$ normalized by $\overline{w'\theta'}_0$ at tower top for unstable runs ($-10 < (z-z_d)/L < -0.5$). The observed pattern is consistent with changing wind direction and the only notable difference is that along-canyon flow leads to higher $\overline{w'\theta'}$ values in the central canyon. This might be due to the fact that heat transfer between the canyon and the air aloft under those conditions is more turbulent within the canyon, whereas in the cross-canyon flow the dispersive flux $\overline{w}''\overline{T}''$ associated with steady-state flow patterns (street canyon vortex) might be more significant.

### 4.5 Dissipation $\epsilon$

The very small eddies involved in the viscous dissipation of TKE cannot be measured directly with sonic anemometers. Instead, the viscous dissipation rate $\epsilon$ was deduced from the inertial subrange (ISR) of streamwise velocity spectra by using Kolmogorov's similarity approach and Taylor's hypothesis (Kaimal and Finnigan 1994), viz.

$$\epsilon = \frac{2\pi n}{\overline{u}} \left( \frac{n S_u(n)}{\alpha_u} \right)^{3/2} \tag{13}$$

where $n$ is the natural frequency, $S_u(n)$ is the spectral energy density of streamwise fluctuations in the given frequency band, and $\alpha_u$ is the corresponding Kolmogorov constant. A correct estimation of $\epsilon$ is only achieved if, (i) an undisturbed ISR with local isotropy exists, and (ii) the Taylor hypothesis is applicable.

**Table 5** Average properties of the flow and of the inertial subrange (ISR) of streamwise velocity spectra relevant for the calculation of $\epsilon$ at U1

| $z/z_h$ | $Re$ | $I_u$ | $S_u/S_w$ | ISR Slope | Err. (%) |
|---|---|---|---|---|---|
| 2.17 | $1.5 \times 10^8$ | 0.45 | 1.14 | −1.63 | 12.8 |
| 1.53 | $6.7 \times 10^7$ | 0.52 | 1.07 | −1.64 | 13.6 |
| 1.23 | $3.1 \times 10^7$ | 0.51 | 1.03 | −1.62 | 14.0 |
| 1.01 | $1.5 \times 10^7$ | 0.48 | 1.15 | −1.60 | 15.2 |
| 0.77 | $1.3 \times 10^7$ | 0.40 | 1.05 | −1.59 | 15.3 |
| 0.25 | $1.4 \times 10^7$ | 0.40 | 1.05 | −1.52 | 19.5 |
| SL | | | 4/3 | −5/3 | |

SL refers to the theoretical surface-layer values. For definitions see text. *Data source*: hourly spectra, November 1, 2001 to July 15, 2002, all stabilities, $n = 3$, 171 h

The first restriction is problematic if $Re < 10^5$ (Tennekes and Lumley 1972), and following the logic of Amiro (1990), Reynolds numbers are estimated by using the integral time scale $\Upsilon_u$ in the streamwise direction and $Re = \overline{u}^2 \Upsilon_u / \nu$. $\Upsilon_u$ was calculated from autocorrelation functions by numerically integrating up to the first zero-crossing. Table 5 shows that Reynolds numbers are on average two order of magnitudes above this threshold.

More problematic might be a contamination of the spectra by small-scale wake production in the high-frequency part of the spectrum. Small-scale wake production is not fully captured in the integral time scale $\Upsilon_u$. From studies in vegetation canopies, it is known that effects such as 'spectral shortcut', a direct bypass of large-scale TKE to small scales by wake generation of small-scale canopy elements (leafs, branches), is expected to alter the spectra in high frequency bands (Finnigan 2000). In the non-vegetated urban canopy at U1, such effects are assumed to be less relevant, since the highest spectral densities at the size of roughness elements ($10^{-2}$ to $10^{-1}$ m$^{-1}$) are larger than at the corresponding wavenumbers in the ISR ($10^{-1}$ to $10^{0}$ m$^{-1}$). Roth et al. (2006) concluded in their spectral analysis of the present dataset at U1 that small-scale turbulence production rates are insignificant compared to the size of the energy input at larger scales in the frequency band used for the calculation of $\epsilon$. This cannot be said for U2 with confidence where trees along the avenue are located close to the lower sonics (A–C).

The second restriction, the applicability of Taylor's Hypothesis, is likely to be the most problematic issue in urban canopies. If temporal variations in a moving frame of reference are large and different wavenumbers are transported at different velocities, the Taylor hypothesis fails (Wyngaard and Clifford 1977). In the urban roughness sublayer, strong $Ps$ and $Pw$ create turbulence intensities $I_u = \sigma_u / \bar{u}$ that are typically around 0.5 (Table 5). Willis and Deardorff (1976) suggest that Taylor's hypothesis becomes inapplicable for $I_u > 0.5$, and additionally, a significant pressure transport may result in different propagation velocities for different wavenumbers. Figure 6 (top) shows in a qualitative view that the inertial subrange of spectra in the urban roughness sublayer and especially in the street canyons are, in contrast to spectra from vegetation canopies, surprisingly 'well behaved' and not significantly different from the surface-layer prediction.

The quantity $\epsilon$ was calculated in the spectral band between 0.1 and 1 s$^{-1}$, identified as the most appropriate bandwidth since higher frequencies are more contaminated by back-folding and limited by instrument path length (Kaimal and Finnigan 1994). The ISR slope was

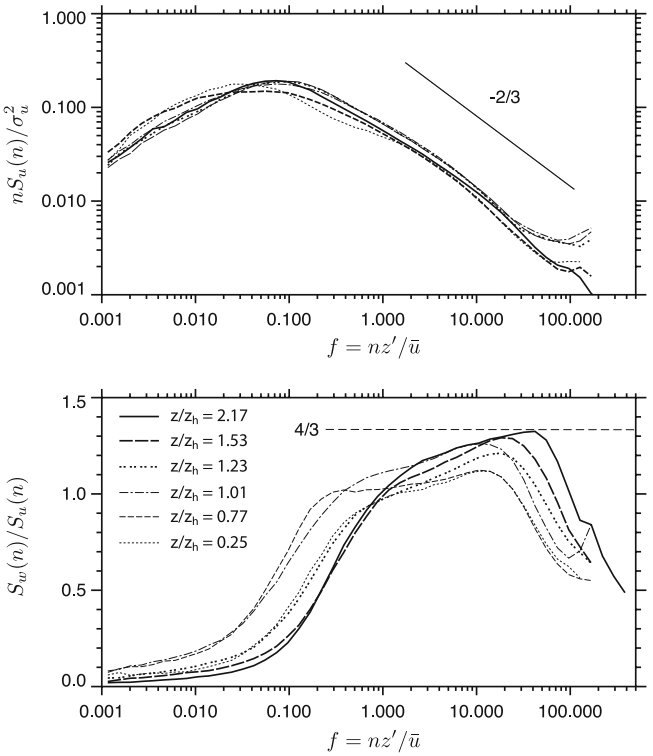


**Fig. 6** *Top*: average streamwise velocity spectra for different heights at U1 with the inertial subrange slope indicated. Frequencies are normalised by local horizontal wind velocity $\bar{u}$ and $z'$ ($z' = (z - z_d)$ above canyon, and $z' = x$ where $x$ is the distance to the nearest wall in the canyon). *Bottom*: ratio $S_w/S_u$ at U1. The *dashed line* indicates the ratio $S_w/S_u$ with local isotropy (4/3). *Data source*: hourly spectra, November 1, 2001 to July 15, 2002, near-neutral conditions only

calculated for each run from the ISR of the $u$ spectra converted to wavenumbers (Table 5 for U1).

For U1, the average ISR slope is slightly lower than the theoretical value of $-5/3$ at all measurement levels, which is interpreted as an indication that small production rates still exist in this range. The ratio $S_w/S_u$ is below the theoretical value of 4/3 for local isotropy (Fig. 6, bottom). Both values suggest an increase of ISR contamination with decreasing height. However, the values show that the contamination levels are still small compared to the energy passed down in the cascade.

The error in Table 5 can be interpreted as the average quality of estimating the $-5/3$ slope fit at all measurement heights, calculated as the root-mean-square deviation of band individual $\epsilon_i$ relative to the average $\epsilon$ of all bands ($n = 13$). These $\epsilon$ values have only been calculated for runs with an ISR slope between $-1.4$ and $-1.8$.

The resulting normalized $\epsilon$ values are highest in the range $1.2 < z/z_h < 1.5$ and decrease in both directions (Fig. 7a). Figure 8b shows the variability of $\epsilon k\, z_h/u_*^3$ for different wind directions at U1. The height of greatest $\epsilon k\, z_h/u_*^3$ significantly varies with wind from different sectors. Immediately above roofs the along-canyon wind shows a lower overall dissipation compared to the cross-canyon situation.

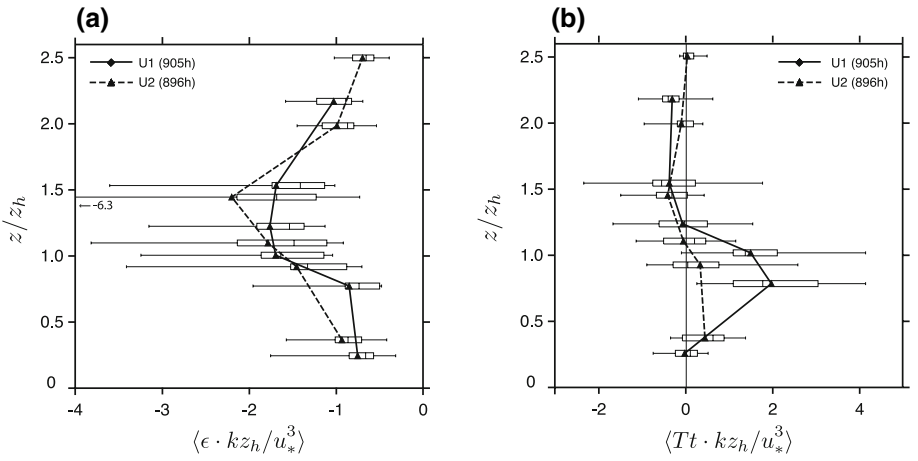


**Fig. 7** Vertical profiles of **a** normalized viscous dissipation rate $\epsilon$ and **b** normalized turbulent transport of TKE. *Data source*: hourly block averages, full operation periods, near-neutral conditions only

Table 6 tests for both sites the prerequisites for local scaling approaches. In a local scaling framework, $\epsilon$ depends only on mechanical (*Ps* and *Pw*) and buoyancy production (*Pb*) at the same height, transport terms and advection are neglected, and the TKE budget is simplified to $\epsilon = Ps + Pw + Pb$. The residual $Ps + Pw + Pb - \epsilon$ is listed in Table 6 and can be regarded as indicating how well local production explains local dissipation at a given height.

At the topmost measurement level at U1, local scaling works adequately and local production nearly balances dissipation; the residual is small compared to other terms (only 3% of $\epsilon$). This supports the fact that local scaling works well here, as reported in numerous field studies that analyzed data measured above roofs using Monin–Obukhov similarity theory (Roth 2000). Closer to the mean roof height at U1 the residual is increasingly positive indicating that more TKE is produced than dissipated. This can be be explained as due to a net export of TKE by transport processes from this region. Turbulence generated in this layer is vertically relocated before it can dissipate ad locum. At the base of the street canyon at U1, $\epsilon$ is significantly higher than locally produced turbulence, suggesting a net import of TKE by transport processes in the lower street canyon.

The situation at U2 is different with regard to the heights but similar in terms of patterns, but complicated by the fact that the sensors are not vertically aligned. At the highest two levels, the residual is small compared to other terms. At $z/z_h = 1.44$ there is less dissipation than production, hence an export of TKE is observed. The cross-over to a positive residual (more dissipated than is locally produced) is found around $z/z_h = 1.2$. However, the mid-canyon level does again suggest a well-balanced budget. At the bottom of the street canyon at U2, the dissipation rate is significantly higher than local production, again suggesting a net import of TKE by transport processes. For both sites, we conclude that any local scaling approach produces inaccurate results at rooftop and at the bottom of the street canyon.

### 4.6 Turbulent Transport *Tt*

We postulated that at roof level and in the street canyon the 'spatially'-averaged TKE budget is not in local equilibrium and locally produced TKE by *Ps*, *Pw* and *Pb* does not equal local $\epsilon$. This indicates that TKE must be vertically relocated by transport processes. Roth and Oke (1993a) suggested in their analysis of a suburban dataset that large organised structures

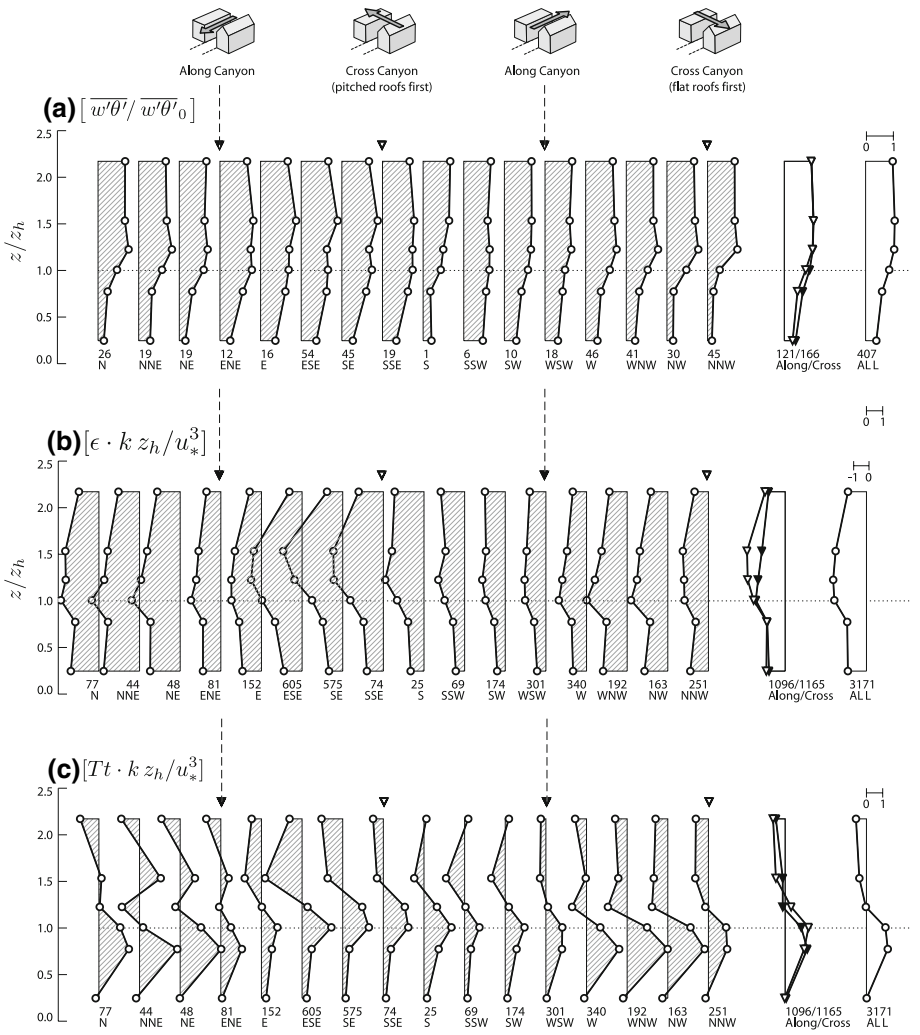


**Fig. 8** Conditionally-averaged profiles of **a** kinematic heat flux $\overline{w'\theta'}$ normalized by kinematic heat flux at tower top $\overline{w'\theta'}_0$ for unstable cases, **b** normalized viscous dissipation rate $\epsilon k\, z_h/u_*^3$ for all cases, **c** normalized turbulent transport of TKE $Tt\, k\, z_h/u_*^3$ for all cases, at U1 for all 16 wind direction classes separately, for conditionally-averaged along and cross-canyon situations, and the average profile of all 16 classes (*right*) according the procedure outlined in Sect. 3.2.3. Numbers above the wind direction labels denote the number of hourly blocks included in the conditionally averaged profiles. *Data source*: hourly block averages, November 1, 2001 to July 15, 2002

are involved in the relocation and transfer of TKE. Feigenwinter and Vogt (2005) sampled coherent structures on a tower in the city of Basel 400 m to the south-east of U1, and conditionally sampled large ejection-sweep sequences detected at three heights simultaneously (36, 50 and 76 m). They concluded that these organised structures show highest normalised fluctuations at the lowest level although they were effectively contributing to $\overline{u'w'}$ and $\overline{w'\theta'}$ at all levels. Christen et al. (2007) applied classical quadrant analysis and a conditional sampling approach to the present dataset at U1. Their results show that large coherent structures

**Table 6** Local production and dissipation at both sites

| | $z/z_h$ | Local production $\langle Ps\rangle + \langle Pw\rangle + \langle Pb\rangle$ | Local dissipation $\langle\epsilon\rangle$ | *Res.* | *Res.*/$\langle\epsilon\rangle$ (%) |
|---|---|---|---|---|---|
| U1 | 2.17 | 1.17 | −1.20 | 0.03 | +3 |
| | 1.53 | 2.32 | −2.01 | −0.31 | −16 |
| | 1.23 | 3.32 | −2.17 | −1.16 | −53 |
| | 1.01 | 2.59 | −2.09 | −0.50 | −24 |
| | 0.77 | 1.01 | −1.25 | 0.25 | +20 |
| | 0.25 | 0.83 | −1.21 | 0.38 | +32 |
| U2 | 2.49 | 0.97 | −0.88 | −0.09 | −11 |
| | 1.98 | 1.20 | −1.22 | 0.02 | +1 |
| | 1.44 | 3.30 | −2.65 | −0.66 | −25 |
| | 1.10 | 1.43 | −2.30 | 0.87 | +38 |
| | 0.92 | 1.95 | −1.91 | −0.04 | −2 |
| | 0.37 | 0.84 | −1.59 | 0.75 | +47 |

*Res.* is the residual of the local processes, i.e. $Res. = \langle Ps\rangle + \langle Pw\rangle + \langle Pb\rangle - \langle\epsilon\rangle$. All terms are normalized by $k\,z_h/u_*^3$ and averaged according Sect. 3.2.3. *Data source*: hourly values, November 1, 2001 to July 15, 2002, all stabilities, $n = 3$, 171 h

of the size of the whole vertical domain of the urban roughness sublayer dominate exchange processes. However, no study directly determined transport terms of the TKE budget in the urban roughness sublayer.

The only transport term that can be measured directly with the current set-up is the turbulent transport term (*Tt*). *Tt* has been approximated based on Eq. 5 using a cubic spline interpolation for the vertical gradient of all three third-order moments and taking a changing fractional volume $\Lambda_a$ with height into account.

In near-neutral runs, on average all three third-order moments of type $\overline{w'u_i'^2}$ contribute to a downward transport of TKE, and greatest $\overline{w'u_i'^2}$ values are found around $z_h$. Figure 7b shows the average profile for the resulting turbulent transport term under neutral conditions. Above $2z_h$, *Tt* is small, however the normalised *Tt* becomes more strongly negative with increasing destabilisation at both sites (Fig. 9). This is mainly an effect of the normalisation by a smaller $u_*^3$.

With decreasing height, *Tt* becomes more important. First, above roofs we find a layer with a net export of TKE. Then at roughly $1.2\,z_h$ at both sites, *Tt* changes from a sink to a source with a net import of TKE in the upper street canyon. In other words, *Tt* qualitatively follows the pattern postulated above by transporting excess TKE from the region above rooftop where shear production prevails ($1.2 < z/z_h < 2$) down into the street canyon ($z/z_h < 1.2$). At U1, *Tt* is the most important source of TKE in the upper canopy for all stabilities (Fig. 9). At the street level, *Tt* is of smaller relevance although the largest TKE import is expected there from the failure of the local scaling approach (Table 6). In the canyon at U2, *Tt* is also positive but less relevant than at U1.

Results reported from model or field studies in vegetation canopies generally suggest a similar pattern. TKE is vertically relocated from the shear region above the vegetation canopy down into the 'low velocity flow' within the canopy (Leclerc et al. 1990; Meyers and Baldocchi 1991; Brunet et al. 1994; Shen and Leclerc 1997).

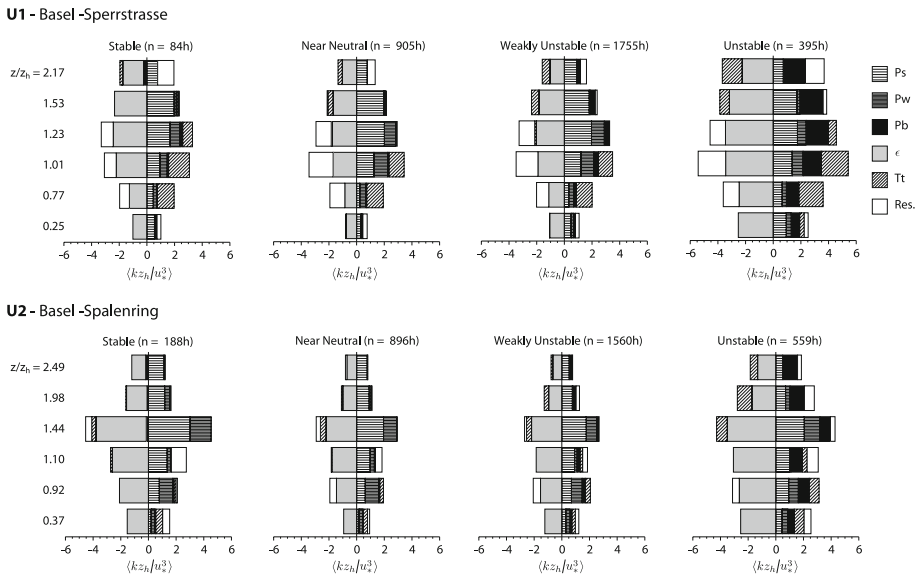


**Fig. 9** Average normalized terms of the directionally-averaged TKE budget at U1 (*top row*) and at U2 (*bottom row*) for different stability classes measured by $\zeta$ at tower top (see Sect. 3.2.3). Shear production *Ps*, wake production *Pw*, buoyancy production *Pb*, viscous dissipation rate $\epsilon$, turbulent transport *Tt* and the residual term. In brackets the number of hourly block averages included in the statistics for each class are indicated. *Data source*: November 1, 2001 to July 15, 2002

**Table 7** Turbulent transport (*Tt*) of TKE and estimation of the dispersive transport (*Td*) of TKE normalised by $kz_h/u_*^3$ for near-neutral conditions at U1

*Data source*: hourly averages, November 1, 2001 to July 15, 2002, near-neutral conditions only, $n = 905$ h

| $z/z_h$ | *Tt* | *Td* | $\lvert Td\rvert/(\lvert Tt\rvert + \lvert Td\rvert)$ |
|---|---|---|---|
| 2.49 | −0.01 | – | – |
| 1.98 | 1.20 | 0.05 | 4% |
| 1.44 | 1.10 | 0.09 | 8% |
| 1.10 | −0.07 | 0.08 | 53% |
| 0.92 | −0.38 | −0.06 | 14% |
| 0.37 | −0.31 | −0.02 | 6% |

## 4.7 Dispersive Transport *Td*

The dispersive term $\overline{u_i' u_i'}''$ in *Td* has been approximated by

$$\frac{\overline{u_i' u_i'}''(z)}{u_*^2} \approx \frac{\overline{u_i' u_i'}(z)}{u_*^2} - \left\langle \frac{\overline{u_i' u_i'}}{u_*^2} \right\rangle (z) \tag{14}$$

and since $\langle \bar{w} \rangle = 0$, we assume that $\bar{w}''(z) = \bar{w}(z)$. This should be considered a lower boundary for *Td*. The estimated dispersive transport term *Td* is summarised in Table 7, and except at 1.01 $z_h$, the dispersive transport has the same sign as the turbulent transport. Because *Td* is typically 10 times less important than *Td*, we neglect this term in the further analysis.

### 4.8 Pressure Transport *Tp*

Pressure transport is likely the most important of the non-measured terms. In the present set-up, no attempts were made to measure pressure transport directly, since measuring turbulent pressure fluctuations in the field is difficult and results are limited (Elliott 1972; Katul et al. 1996; Wilczak and Bedard 2004). In the present work, the residual term is interpreted as pressure transport. Likely in many individual runs, advection is the dominating term in the residual, but the spatial averaging procedure will, at least partially, offset advection due to symmetry assumptions as suggested in Fig. 10. Still, results of the residual term have to be interpreted with caution since a residual includes all errors of the measurements and all assumptions and simplifications made so far. Results from the large-eddy simulation study of Dwyer et al. (1997) suggest that stability affects *Tp* by increasing it substantially under unstable conditions.

The analysis of the residual term at U1 suggests that pressure disturbances are primarily created in the region around rooftop and in the upper street canyon. Pressure transport likely relocates TKE from the layer at rooftop and exports it up to $z/z_h > 2$ and also down into the very bottom of the street canyon (Fig. 9, top row). This pattern is consistently found under all stability regimes, suggesting that stability at tower top does not significantly control the partitioning between terms. Overall stability mainly affects the layers well above the roofs where pressure transport and turbulent transport are always of opposite sign. This is an effect reported from observations in the surface layer (McBean and Elliott 1975). In relative numbers, the residual is an important source only in the lowest part of the street canyon where the estimation of *Pw* is associated with largest uncertainties, and turbulence produced by moving vehicles *Pt* might play a role. In general, the observed pattern at U1 where pressure transport is a sink at rooftop and a source in the lower street canyon is in qualitative agreement with the few indirect measurements of the pressure term in vegetation canopies (Maitani and Seo 1985; Shaw et al. 1990) and with numerical model results (Shen and Leclerc 1997; Dwyer et al. 1997). At U2, the residual term provides a less clear picture (Fig. 9, bottom row), and is likely due to the fact that the same vertical profile was not probed. Still, the residual term is surprisingly small for all stabilities at U2.

### 4.9 Turbulence Produced by Moving Vehicles *Pt*

At the bottom of the street canyon, the traffic-produced TKE is part of the residual term, and it is difficult to separate *Pt* from other non-measured processes such as *Tp* or advection. At U1, the daily traffic load was measured at 2,000 vehicles per day with a peak in the late afternoon at 170 vehicles per hour (Vogt et al. 2006). Average vehicle speed was 7.8 $\mathrm{m\,s^{-1}}$. No correlation is found between the magnitude of the residual term and the traffic load at U1. The moderate traffic load, a speed limit (8.3 $\mathrm{m\,s^{-1}}$), and the one-way traffic might explain why there was no determinable correlation between the residual term and traffic load in the street canyon.

### 4.10 Implications on the Concept of Local Scaling

In the urban roughness sublayer, and especially in the street canyon, both Reynolds stress $\overline{u'w'}$ (Fig. 5b) and kinematic heat flux $\overline{w'\theta'}$ (Fig. 8a) decrease with height. Therefore, velocity variances do not scale with a global $u_*$ and kinematic surface heat flux $\overline{w'\theta'}_0$ as they do in the inertial sublayer. To overcome this limitation, Högström et al. (1982) introduced the local

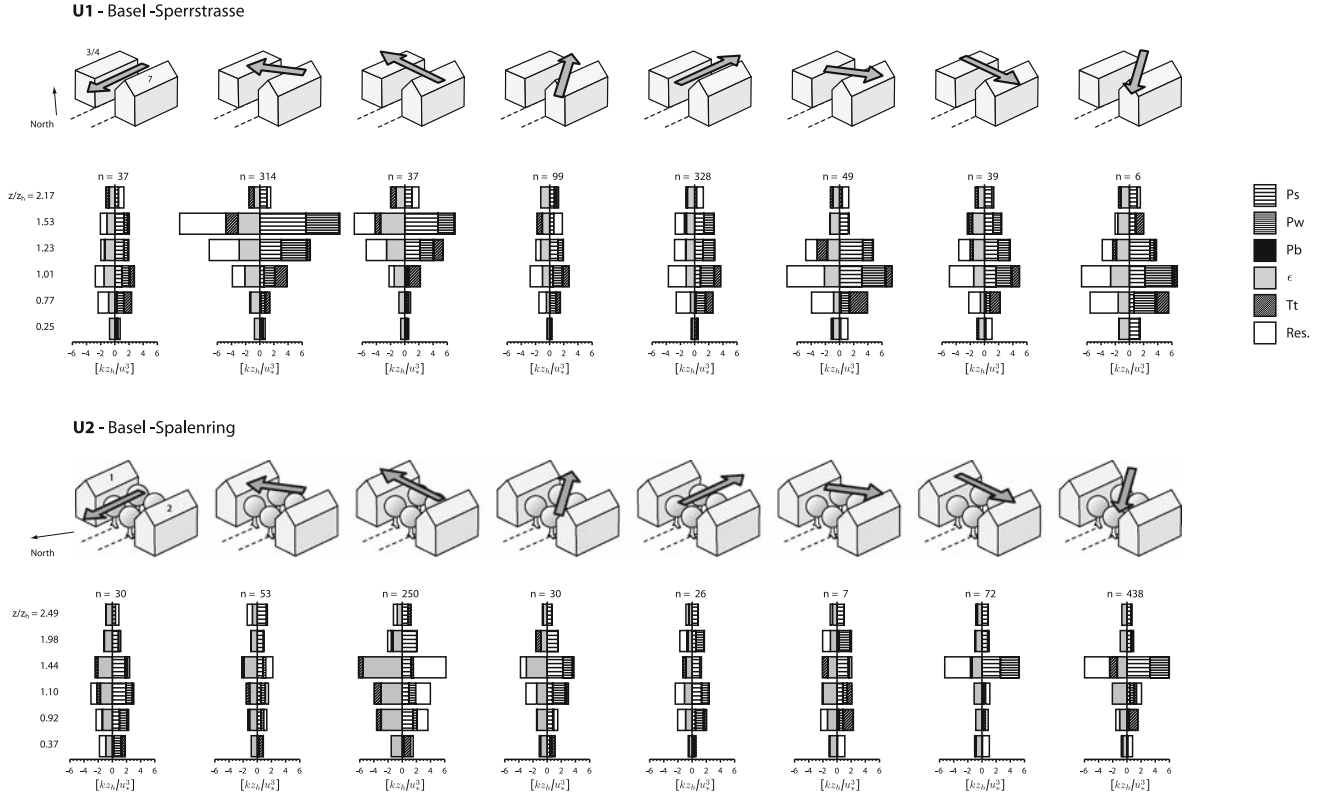


**Fig. 10** Conditionally-averaged terms of the TKE budget at U1 (*top row*) and at U2 (*bottom row*) for different wind directions relative to the canyon axis, for neutral conditions only. Abbreviations see Fig. 9. *Data source*: neutral conditions, November 1, 2001 to July 15, 2002

scaling concept, which has been widely used in urban turbulence studies. In this concept, the scaling velocity is explicitly local, i.e. derived from $\overline{u'w'}(z)$, and the same is true for the local Obukhov length $L_{\mathrm{loc}}$. To account for rotating wind with height, an effect due to channelling of air flow in street canyons, velocity variances are typically calculated incorporating local $\overline{u'w'}(z)$ and $\overline{v'w'}(z)$:

$$a_i(z) = \sigma_i(z) \Big/ \left(\overline{u'w'}^2(z) + \overline{v'w'}^2(z)\right)^{1/4} \tag{15}$$

with $i = \{u, v, w\}$. Numerous previous studies above urban surfaces (but not in street canyons) demonstrated that locally scaled velocity variances of the form $a_i = \sigma_i/u_*$ do not differ significantly from the prediction of Monin–Obukhov similarity theory (see e.g. review by Roth 2000). The rate of local production of TKE and the frequency of the produced eddies determine the integral variance, i.e. strong excursions are related to large structures, which contain more energy and have a longer life span. A well-behaved shape of the velocity spectra links life span and integral energy to the rate of local dissipation. This argumentation agrees with classical Monin–Obukhov similarity theory. Note that turbulent transport and pressure transport are neglected in both local and global scaling approaches. Whenever transport terms *Tt* and *Tp* become relevant, transport processes can export TKE before it is dissipated ad locum. This alters the ratio between TKE and local production and hence lowers any scaled velocity variance $a_i$ in layers with a net export of TKE and increases them in layers with a net import of TKE. This explanation for differences in integral statistics has been suggested by Roth and Oke (1993b).

In the analysis of the TKE budget equation we concluded that at the tower tops of U1 and U2 *Tp* is counter-directed to *Tt*. In near-neutral conditions, the transport terms are small compared to shear production (Fig. 9), and supporting the partial success of the local scaling approach in the urban roughness sublayer well above mean building height, at least under near-neutral conditions. The differences of the scaled velocity variances closer to the roofs reported in other studies over urban surfaces of similar density (Rotach 1993a; Feigenwinter et al. 1999) might be explained by missing the incorporation of transport processes in the local scaling approach.

Close to the inflexion point of the wind profile, the neutral limit of $a_u$ is indeed significantly lower compared to values higher up where surface-layer values are reached. This reflects the export of TKE by *Tt* (Fig. 11a). Note, however, that the neutral limit of $a_u$ is still higher than values observed in plane mixing layers, which are typically $a_u \approx 1.7$ (Raupach et al. 1996). Individual values from selected flow sectors reach the plane mixing layer limit; for example, flow from the north-north-west over the flat roofs first at U1 has an average neutral limit of $a_u = 1.69$ at $z_h$ and flow from the south-east shows an average value of $a_u = 1.73$ at $1.53\,z_h$ (this height corresponds to the top of the pitched roof labelled '7' in Fig. 1).

TKE created at roof level does not remain in this layer for long and is transported down into the street canyon by organised structures before it can dissipate. This turbulent transport process (*Tt*) enhances $\sigma_u(z)$ in the street canyon where $\overline{u'w'}$ and $\overline{v'w'}$ are small, explaining why neutral limits of velocity variances are often considerably higher in the street canyon compared to surface-layer predictions when using a local scaling approach.

For the locally scaled lateral variance $a_v$, neutral limits fit more adequately to surface-layer predictions (Fig. 11b). Similarly to $a_u$, $a_v$ is also characterized by a slight reduction close to the inflexion point of the wind profile and in the upper street canyon. In the street canyon, likely channelling of the flow into the canyon reduces lateral deviations, and therefore the lateral component is not substantially enhanced.

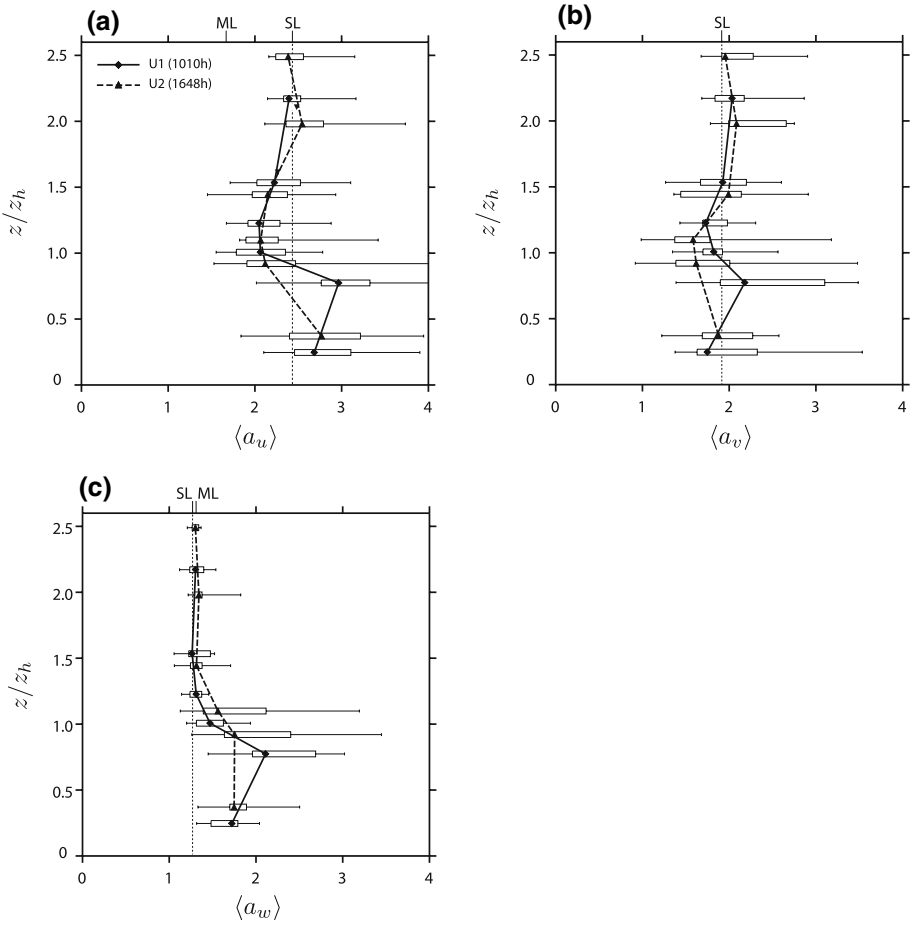


**Fig. 11** Profiles of the neutral limits of locally scaled velocity variances **a** $a_u$, **b** $a_v$, and **c** $a_w$. SL and ML denote the neutral surface layer and the neutral plane mixing layer limits, respectively. *Data source*: hourly block averages, full operation periods

For $a_w$, profiles show good agreement with the surface-layer values down to $1.2\,z_h$ (Fig. 11c). In both street canyons, the neutral limit increases significantly below $1.2\,z_h$ towards a maximum at $0.8\,z_h$. Here, in the middle street canyon, two processes enhance $a_w$, the turbulent downward transport of TKE and the mean flow field. The mean flow field often rotates initial streamwise fluctuations into vertical motion, i.e. energy contained in $\sigma_u$ can be transformed into $\sigma_w$ by large-scale stationary or semi-stationary eddies such as the classical street-canyon vortex. At street level, $a_w$ again decreases at both sites. Here again the streamwise component dominates the mean flow, so energy contained in $\sigma_w$ in the upper part of the street canyon is rotated back into $\sigma_u$.

## 5 Summary and Conclusions

In Fig. 10 the average profiles of the terms of the TKE budget at the present two urban sites are summarized. Data are conditionally averaged for different sectors of wind direction and

only near-neutral cases are employed in this summary. With the term 'roughness sublayer' we inherently associate the fact that individual values of any property strongly depend on location and specific flow configuration. Indeed, profiles measured at the two towers show a strong dependence on the direction of the ambient flow relative to the local street canyon. This has been already illustrated in the conditionally-averaged profiles for different terms in Figs. 5 and 8. 'Horizontally-averaged' profiles were retrieved by averaging these ensemble profiles over different wind directions according to the procedure outlined in Sect. 3.2.3. These 'horizontally-averaged' profiles show a surprisingly similar shape at the two towers (Fig. 9), and is interpreted as an indication that they represent general processes in the urban roughness sublayer or at least in typical street canyons. However, we must keep in mind that a true spatial average cannot be retrieved from a full-scale environment using measurements taken in a single vertical array. The postulated convergence between the true spatial average and the average retrieved using the approach of averaging over all wind directions cannot strictly be verified using data from the present experiment. The similarity between the two towers in the lower part might also reflect the fact that at both sites, measurements were made in a rather similar urban geometry. All 'horizontally-averaged' terms should be discussed with this fundamental restriction in mind.

Conditionally-averaged profiles for different wind directions such as shown in Fig. 10 typically indicate that production and dissipation are significantly smaller for cases with wind along the canyons. Cross-canyon flow creates stronger gradients with more intense local production of TKE by *Ps* and *Pw*.

### 5.1 In the Street Canyons

Turbulent shear production and turbulent buoyancy production are both of minor importance in the street canyon. Here, TKE is mainly imported by large coherent structures (sweeps) from rooftop level. In the upper canyon, wake production *Pw* is important. The analysis of the residual gives some evidence that under certain flow configurations TKE may be removed from the upper part of the urban canopy and transported down to the very bottom of the street canyon through the process of pressure transport.

### 5.2 At Rooftops

Around rooftop, the profiles of $\overline{u}$, $\overline{u'w'}$ and $\overline{u_i'^2 w'}$ are all characterised by strong vertical gradients. Here, both shear production *Ps* and wake production *Pw* are significant sources of TKE. A notable amount of TKE is exported by sweeps into the upper street canyon and by ejections into the inertial sublayer above through turbulent transport *Tt*. Further, there is evidence that pressure transport may remove TKE from the layer at rooftop, and in general, the layer at rooftop can be seen as an export region for TKE. As a consequence, $\epsilon$ is lower than locally produced turbulence. This explains why neutral limits of horizontal velocity variances are significantly smaller in the roof layer than are predicted by local surface-layer scaling.

### 5.3 Above Roofs

Above the highest roofs, all flow characteristics gradually approach surface-layer values. Turbulent transport and pressure transport are of opposite sign and decrease relative to shear and buoyancy production. Also wake production decreases with height. Therefore, the local

scaling approach does work reasonably well in the upper part of the urban roughness sublayer i.e. above the highest roofs.

### 5.4 Implications

The observations suggest that models and approaches using surface-layer theory with either classical or modified (urban) constants are inadequate and fail in the lower urban roughness sublayer (i.e. close to roofs and within the canopy). Therefore, alternative approaches and simplifications are needed. These alternative approaches must take into account the vertical relocation of TKE by coherent structures, wake production of TKE and likely pressure transport. In the last 15 years, turbulent exchange in vegetation canopies has been successfully addressed with the help of higher order closure schemes and the *plane mixing-layer analogy* (Raupach et al. 1989, 1996; Finnigan 2000). It is beyond the scope of this paper to discuss potential success or failure of different models and approaches in an urban context. However, at least qualitatively the present profiles of TKE budget terms indeed are similar in many respects to the features found in vegetation canopies. The two presented urban datasets show an inflected velocity profile, strongest gradients at $z_h$, significant wake production in the upper canopy, non-negligible turbulent transport terms, and the importance of coherent structures. This suggests that a number of the observed characteristics are driven by processes that are likely valid for flow over rough and porous land-atmosphere interfaces in general.

**Acknowledgements** The Swiss Federal Office for Education and Science provided funding of this study (Grant C00.0068). The authors would like to express their thanks to C. Feigenwinter (University of Basel, Switzerland), M. Roth (National University of Singapore, Singapore), E. van Gorsel (CSIRO, Canberra, Australia) for their valuable contributions to program code and discussions. Authors also wish to thank the anonymous reviewers, who provided very helpful comments for the final manuscript. We are indebted to a large group of people who did a great job contributing to the challenging set-up and maintenance of the towers and instruments. But the experimental set-up would have never been possible without the full support of the authorities and the inhabitants of the City of Basel. Additional site documentation including photos and drawings of the towers can be found on the BUBBLE web site http://pages.unibas.ch/geo/mcr/Projects/BUBBLE/.

## References

Amiro BD (1990) Drag coefficients and turbulence spectra within three boreal forest canopies. Boundary-Layer Meteorol 52:227–246

Belcher SE (2005) Mixing and transport in urban areas. Philos Trans R Soc A 363:2947–2968

Britter RE, Hanna SE (2003) Flow and dispersion in urban areas. Annu Rev Fluid Mech 35:469–496

Brunet Y, Finnigan JJ, Raupach MR (1994) Wind-tunnel study of air-flow in waving wheat—single-point velocity statistics. Boundary-Layer Meteorol 70:95–132

Ca VT, Ashie Y, Asaeda T (2002) A k-epsilon turbulence closure model for the atmospheric boundary layer including urban canopy. Boundary-Layer Meteorol 102:459–490

Cheng H, Castro IP (2002) Near wall flow over urban-like roughness. Boundary-Layer Meteorol 104:229–259

Christen A (2005) Atmospheric turbulence and surface energy exchange in urban environments—results from the Basel Urban Boundary Layer Experiment (BUBBLE), vol 11 of stratus. Institute of Meteorology, Climatology and Remote Sensing, Department of Geosciences, University of Basel. 3-85977-266-X

Christen A, Vogt R (2004) Energy and radiation balance of a Central European city. Int J Climatol 24: 1395–1421

Christen A, van Gorsel E, Vogt R (2007) Coherent structures in urban roughness sublayer turbulence. Int J Climatol 27:1955–1968

Coceal O, Thomas T, Castro I, Belcher S (2006) Mean flow and turbulence statistics over groups of urban-like cubical obstacles. Boundary-Layer Meteorol 121:491–519

Dwyer MJ, Patton EG, Shaw RH (1997) Turbulent kinetic energy budgets from a large-eddy simulation of airflow above and within a forest canopy. Boundary-Layer Meteorol 84:23–43

Elliott JA (1972) Microscale pressure fluctuations measured within the lower atmospheric boundary layer. J Fluid Mech 53:351–383
Feddersen B (2005) Wind tunnel modelling of turbulence and dispersion above tall and highly dense urban roughness, vol 15934 of diss. ETH. Swiss Federal Institute of Technology (ETH), Zürich
Feigenwinter C, Vogt R (2005) Detection and analysis of coherent structures in urban turbulence. Theor Appl Climatol 81:219–230
Feigenwinter C, Vogt R, Parlow E (1999) Vertical structure of selected turbulence characteristics above an urban canopy. Theor Appl Climatol 62:51–63
Finnigan JJ (2000) Turbulence in plant canopies. Annu Rev Fluid Mech 22:519–557
Frenzen P, Vogel CA (2001) Further studies of atmospheric turbulence in layers near the surface: scaling the TKE budget above the roughness sublayer. Boundary-Layer Meteorol 99:173–206
Garratt JR (1994) The atmospheric boundary layer. Cambridge University Press, UK, 316 pp
Grimmond CSB, Oke TR (1999) Aerodynamic properties of urban areas derived from analysis of surface form. J Appl Meteorol 38:1262–1292
Högström U, Bergström H, Alexandersson H (1982) Turbulence characteristics in a near-neutrally stratified urban atmosphere. Boundary-Layer Meteorol 23:449–472
Kaimal JC, Finnigan JJ (1994) Atmospheric boundary layer flows—their structure and measurement. Oxford University Press, New York, 289 pp
Kastner-Klein P, Fedorovich E, Rotach MW (2001) A wind-tunnel study of organised turbulent motions in urban street canyons. J Wind Eng Ind Aerodyn 89:849–861
Katul GG, Albertson JD, Hsieh CI, Conklin PS, Sigmon JT, Parlange MB, Knoerr KR (1996) The 'inactive' eddy motion and the large-scale turbulent pressure fluctuations in the dynamic sublayer. J Atmos Sci 6:2512–2524
Leclerc MY, Beissner KC, Shaw RH, den Hartog G, Neumann HH (1990) The influence of atmospheric stability on the budgets of the Reynolds stress and turbulent kinetic energy within and above a deciduous forest. J Appl Meteorol 29:916–933
Maier W (2005) 10 Jahre 3D-Stadtmodell Kanton Basel-Stadt. Geomat Schweiz 6:348–350
Maitani T, Seo T (1985) Estimates of velocity-pressure and velocity pressure gradient interactions in the surface layer above plant canopies. Boundary-Layer Meteorol 33:51–60
Martilli A, Santiago JL (2007) CFD simulation of airflow over a regular array of cubes. Part II: analysis of spatial average properties. Boundary-Layer Meteorol 122:635–654
McBean GA, Elliott JA (1975) Vertical transports of kinetic-energy by turbulence and pressure in boundary-layer. J Atmos Sci 32:753–766
McMillen RT (1988) An eddy correlation technique with extended applicability to non-simple terrain. Boundary-Layer Meteorol 43:231–245
Meyers TP, Baldocchi DD (1991) The budgets of turbulent kinetic energy and Reynolds stress within and above a deciduous forest. Agric For Meteorol 53:207–222
Oikawa S, Meng Y (1995) Turbulence characteristics and organized motion in a suburban roughness sublayer. Boundary-Layer Meteorol 74:289–312
Poggi D, Katul GG, Albertson JD (2004) Momentum transfer and turbulent kinetic energy budgets within a dense model canopy. Boundary-Layer Meteorol 111:589–614
Press WH, Teukolsky SA, Vetterling WT, Flannery BP (1994) Numerical recipes in C—the art of scientific computing, 2nd edn. Cambridge University Press, Cambridge
Raupach MR, Shaw RH (1982) Averaging procedures for flow within vegetation canopies. Boundary-Layer Meteorol 22:79–90
Raupach MR, Coppin PA, Legg BJ (1986) Experiments on scalar dispersion within a model-plant canopy. I. The turbulence structure. Boundary-Layer Meteorol 35:21–52
Raupach MR, Finnigan JJ, Brunet Y (1989) Coherent eddies in vegetation canopies. In: Fourth proc. Australasian conf. heat mass transfer, Christchurch, New Zealand, May 9–12 1989, pp 75–90
Raupach MR, Finnigan JJ, Brunet Y (1996) Coherent eddies and turbulence in vegetation canopies: the mixing-layer analogy. Boundary-Layer Meteorol 78:351–382
Rotach MW (1993a) Turbulence close to a rough urban surface. II. Variances and gradients. Boundary-Layer Meteorol 66:75–92
Rotach MW (1993b) Turbulence close to a rough urban surface. I. Reynolds stress. Boundary-Layer Meteorol 65:1–28
Rotach MW (1999) On the influence of the urban roughness sublayer on turbulence and dispersion. Atmos Environ 33:401–408
Rotach MW, Gryning SE, Batchvarova E, Christen A, Vogt R (2004) Pollutant dispersion close to an urban surface—the BUBBLE tracer experiment. Theor Appl Climatol 87:39–56

Rotach MW, Vogt R, Bernhofer C, Batchvarova E, Christen A, Clappier A, Feddersen B, Gryning SE, Martucci G, Mayer H, Mitev V, Oke TR, Parlow E, Richner H, Roth M, Roulet YA, Ruffieux D, Salmond J, Schatzmann M, Voogt J (2005) BUBBLE—an urban boundary layer meteorology project. Theor Appl Climatol 81:231–261

Roth M (2000) Review of atmospheric turbulence over cities. Q J Roy Meteorol Soc 126:941–990

Roth M, Oke TR (1993a) Turbulent transfer relationships over an urban surface. I. Spectral characteristics. Q J Roy Meteorol Soc 119:1071–1104

Roth M, Oke TR (1993b) 'Turbulent transfer relationships over an urban surface. II. Integral statistics. Q J Roy Meteorol Soc 119:1105–1120

Roth M, Salmond JA, Satyanarayana ANV (2006) Methodological considerations regarding the measurement of turbulent fluxes in the urban roughness sublayer: the role of scintillometry. Boundary-Layer Meteorol 121:351–375

Sabatino SD, Kastner-Klein P, Berkowicz R, Britter RE, Fedorovich E (2003) The modelling of turbulence from traffic in urban dispersion models. I. Theoretical considerations. Environ Fluid Mech 3:129–143

Shaw RH, Paw KT, Zhang XJ, Gao W, den Hartog G, Neumann HH (1990) Retrieval of turbulent pressure fluctuations at the ground surface beneath a forest. Boundary-Layer Meteorol 50:319–338

Shen SH, Leclerc MY (1997) Modelling the turbulence structure in the canopy layer. Agric For Meteorol 87:3–25

Tennekes H, Lumley JL (1972) A first course in turbulence. MIT Press, Cambridge, 300 pp

Vogt R, Christen A, Rotach MW, Roth M, Satyanarayana ANV (2006) Temporal dynamics of $CO_2$ fluxes and profiles over a Central European city. Theor Appl Climatol 84(1–3):117–126

Wilczak JM, Bedard AJ (2004) A new turbulence microbarometer and its evaluation using the budget of horizontal heat flux. J Atmos Ocean Technol 21:1170–1181

Wilczak JM, Oncley SP, Stage SA (2001) Sonic anemometer tilt correction algorithms. Boundary-Layer Meteorol 99:127–150

Willis GE, Deardorff JW (1976) On the use of Taylor's hypothesis for diffusion in the mixed layer. Q J Roy Meteorol Soc 102:817–822

Wyngaard JC, Clifford SF (1977) Taylor's hypothesis and high frequency turbulence spectra. J Atmos Sci 34:922–929